

GLOBAL-MEAN VERTICAL TRACER MIXING IN PLANETARY ATMOSPHERES

XI ZHANG¹ AND ADAM P. SHOWMAN²

¹Department of Earth and Planetary Sciences, University of California Santa Cruz, CA 95064 and
²Department of Planetary Sciences and Lunar and Planetary Laboratory, University of Arizona, AZ 85721

submitted to the ApJ

Abstract

Most current atmospheric chemistry models and haze and cloud formation models for solar system planets and extra-solar planets adopt a one-dimensional (1D) chemical-diffusion approach to approximate the global-mean vertical tracer transport. The physical underpinning of the key parameter in this framework, eddy diffusivity, is usually obscure. Here we analytically and numerically investigate vertical tracer transport in a 3D stratified atmosphere and predict the effective 1D eddy diffusivity K_{eff} , commonly called K_{zz} in 1D models. We find that K_{eff} strongly depends on the large-scale circulation strength, horizontal mixing due to eddies and waves and local tracer sources and sinks due to chemistry and microphysics. We also find that the global-mean vertical tracer mixing does not always behave diffusively. If the chemical and microphysical processes are non-uniformly distributed across the globe—for example, photochemistry or cloud formation on tidally locked planets—a significant non-diffusive component might lead to a negative K_{eff} under the diffusive assumption in some situations. Even in the diffusive regime, the traditional assumption in the current 1D models that all chemical species are transported via the same eddy diffusivity generally breaks down. A key point is that different chemical species in a single atmosphere should in principle have different eddy diffusion profiles, because of the effect of chemistry on vertical mixing rates. We find that K_{eff} increases with tracer chemical lifetime and circulation strength but decreases with horizontal eddy mixing efficiency. Numerical simulations of 2D and 3D tracer transport on fast-rotating zonal-symmetric planets and tidally locked exoplanets confirm our analytical K_{eff} theory over a wide parameter space. Using species-dependent eddy diffusivity, we provide a new analytical theory of the dynamical quenching points for disequilibrium tracers on tidally locked planets from first principles.

Subject headings: planetary atmospheres - eddy mixing - tracer transport - methods: analytical and numerical

1. INTRODUCTION

The spatial patterns of atmospheric tracers such as chemical species, haze and cloud particles are significantly influenced by atmospheric transport. For most planets in the solar system, the horizontal variations of tracers are usually much smaller than their vertical variations. For extra-solar planets, the horizontal distributions of tracers are not well resolved by observations. The global-mean vertical tracer distribution is the primary focus in most chemistry and cloud models. Vertical transport by large-scale atmospheric circulation and wave breaking leads to a tracer profile that deviates from its chemical or microphysical equilibrium. One example is the “quenching” phenomenon in the atmospheres of giant planets and close-in exoplanets where the gas tracer concentrations (e.g., CO on Jupiter) in the upper atmosphere are not in their local chemical equilibrium, but instead are dominated by strong vertical tracer mixing from the deeper atmosphere. As a result, the observed tracer abundance in the upper atmosphere is “quenched” at an abundance corresponding to the chemical-equilibrium abundance at the location where the tracer chemical timescale is equal to the vertical mixing timescale. This disequilibrium “quenching effect” has a significant influence on the interpretation of observed spectra of planetary atmospheres (e.g., Prinn & Owen 1976, Prinn & Barshay 1977, Smith 1998, Cooper

& Showman 2006, Visscher & Moses 2011).

Investigation of global-mean vertical tracer distribution could be simplified to a one-dimensional (1D) problem. However, because atmospheric tracer transport is intrinsically a three-dimensional (3D) process, parameterization of the 3D transport in a 1D vertical transport model is tricky. Most chemistry models for solar system planets (e.g., Allen et al. 1981, Krasnopolsky & Parshev 1981, Yung et al. 1984, Nair et al. 1994, Moses et al. 2005, Lavvas et al. 2008, Zhang et al. 2012, Wong et al. 2017, Moses & Poppe 2017) and exoplanets (e.g., Moses et al. 2011, Line et al. 2011, Hu et al. 2012, Tsai et al. 2017) adopt a 1D chemical-diffusion approach. Most haze and cloud formation models on planets and brown dwarfs assume the vertical particle transport behaves in a diffusive fashion as well (e.g., Turco et al. 1979, Ackerman & Marley 2001, Helling et al. 2008, Gao et al. 2014). This type of 1D framework originated in the Earth atmospheric chemistry literature but gradually faded out since the 1990’s because it is not sufficient to simultaneously explain the distributions of all the species from observations (Holton 1986) and when the 3D distributions of multiple tracers are well determined by satellite observations from space. At the moment, this 1D framework is still very useful in planetary atmospheric studies. Although only a crude approximation, 1D models have succeeded in explaining the observed global-averaged vertical profiles of many chemical species and particles on planets. =

In the 1D chemical-diffusion framework, the strength

¹ Correspondence to be directed to xiz@ucsc.edu

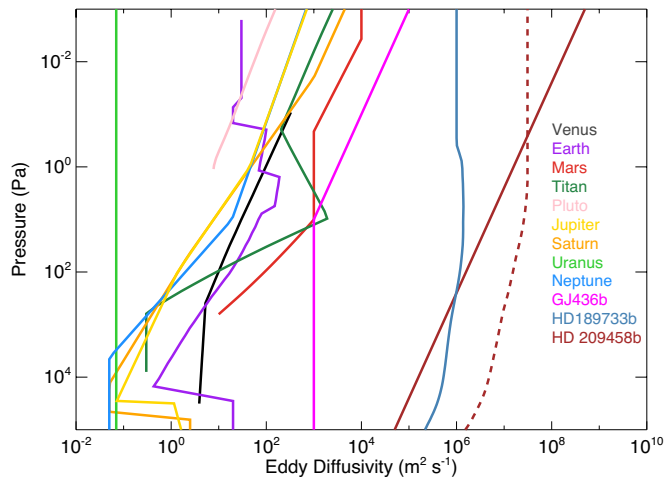


FIG. 1.— Vertical profiles of eddy diffusivity in typical 1D chemical models of planets in and out of the solar system. Sources: Zhang et al. (2012) for Venus, Allen et al. (1981) for Earth, Nair et al. (1994) for Mars, Li et al. (2015) for Titan, Wong et al. (2017) for Pluto, Moses et al. (2005) for Jupiter, Saturn, Uranus and Neptune, Moses et al. (2013) for GJ436b and Moses et al. (2011) for HD189733b and HD209458b. For HD209458b, we show eddy diffusivity profiles assumed in a gas chemistry model (dashed, Moses et al. 2011) and that derived from a 3D particulate tracer transport model (solid, Parmentier et al. 2013).

of the vertical diffusion is characterized by a parameter called eddy diffusivity or eddy mixing coefficient². The 1D effective eddy diffusivity K_{eff} is often determined empirically by fitting the observed vertical tracer profiles. K_{eff} on important planets exhibit vertical profiles and magnitude varying across more than eight orders of magnitude (Fig. 1), implying different vertical transport efficiencies from planet to planet. Since all 3D dynamical effects have been lumped into a single eddy diffusivity, the specific dynamical mixing mechanisms that lead to a particular vertical profile of K_{eff} are often obscure. If the atmosphere is convective, then using the traditional Prandtl mixing length theory (e.g., Prandtl 1925, Smith 1998, Bordwell et al. 2018), one can formulate K_{eff} as a product of a convective velocity and a typical vertical length scale in a turbulent medium. But this formalism fails when the atmosphere is stably stratified. In the low-density middle and upper atmosphere such as Earth’s mesosphere, the vertically propagating gravity waves could break and also lead to a strong vertical mixing of the chemical tracers. Lindzen (1981) parameterized the eddy diffusivity from the turbulence and stress generated in breaking gravity and tidal waves (also see discussion in Strobel 1981, Strobel et al. 1987). In a stratified atmosphere such as Earth’s stratosphere, tracer transport is subjected to both a large-scale overturning circulation and the vertical wave mixing (Hunten 1975, Holton 1986), but whose relative importance depend on altitude and many other factors and may differ from planet to planet. Although there are several 3D chemical-transport simulations in planetary atmospheres with simplified chemical and cloud schemes (e.g., Lefèvre et al. 2004, Lefèvre et al. 2008, Marcq & Lebonnois 2013, Stolzenbach et al. 2015, Cooper & Showman 2006, Par-

² Conventionally, 1D tracer transport models call this global-mean eddy diffusivity as K_{zz} . Here we call it K_{eff} because later in this study we will use K_{zz} as the vertical eddy diffusivity in the 2D (latitude-pressure) tracer transport model.

mentier et al. 2013, Charnay et al. 2015b, Lee et al. 2016, Drummond et al. 2018), a thorough understanding of the physical basis of global-mean vertical tracer transport and K_{eff} using both analytical theory and 3D numerical simulations is still lacking.

In this study we aim to reexamine this conventional diffusion framework. Does the global-mean vertical tracer transport always behave diffusively? If not, under what regimes is diffusion a good assumption and under what regime it is not applicable? In the diffusive regime, how does this K_{eff} depend on tracer sources and sinks and atmospheric dynamics? More fundamentally, how can we achieve a more physically based parameterization of K_{eff} from first principles? One of the conventional assumptions in the existing framework used in current planetary models is that all tracers, in spite of their different chemical lifetimes or particle microphysical/settling timescales, are simulated using the same eddy diffusivity profile K_{eff} . In the real atmosphere, the tracer distribution is controlled by the 3D dynamical and chemical/microphysical processes. A coupling feedback between the chemistry and vertical transport is expected. In fact, it has been noticed in the Earth community (e.g., Holton 1986), in the presence of meridional (latitudinal) transport in the stratospheres, the derived effective eddy diffusivity as a global-mean transport coefficient could have a strong dependence on the tracer lifetime, and thus its chemical/microphysical sources and sinks. On the other hand, Parmentier et al. (2013) studied simple passive cloud tracers using a 3D dynamical model, and showed that the 1D effective eddy diffusivity on hot Jupiters does not exhibit a significant dependence on tracer sinks. This puzzle has not been satisfactorily solved.

In this study we will investigate the tracer transport on both solar system planets and tidally locked exoplanets. We primarily focus on stratified atmospheres such as the stratosphere on solar-system planets or the observable atmospheres (photospheres and above) on highly irradiated exoplanets where most of the chemical tracers and haze/clouds are observed, and which are expected to be stably stratified. The tracer transport in a stratified atmosphere is primarily dominated by large-scale overturning circulation instead of convective mixing, which might be intrinsically different from that in the troposphere or convective interior. In the following sections, we will first elaborate the underlying physics of tracer transport in a global-averaged sense and construct a first-principles estimate of K_{eff} . Then we will use a 2D chemical-transport model to study a 2D meridional circulation system on fast-rotating planets and the behaviors of the associated K_{eff} . A 3D general circulation model with passive tracers are then used to understand the atmospheres on tidally locked exoplanets under two typical scenarios: tracers that are transported from the deep atmosphere and that are produced in the upper atmospheres via photochemistry or ion chemistry. We conclude this study with several key statements and a brief discussion on the effect of vertically propagating gravity waves on the vertical transport of tracers.

2. THEORETICAL BACKGROUND

2.1. Nature of the problem

In a stratified atmosphere, tracers tend to be mixed upward by the large-scale overturning circulation if there is a correlation on an isobar between tracer abundance and vertical velocity: if the tracer abundance is high where the vertical velocity is upward, or if the tracer abundance is low where the vertical velocity is downward, tracer is mixed upward (Fig. 2). This implies that the net vertical mixing of tracer over the globe depends crucially on horizontal variations of the tracer on isobars and on their correlation with the vertical velocity field (Holton 1986). It is the correlation that determines the strength of the global-mean net vertical tracer transport. If the tracer distribution is initially horizontally uniform across the globe with a vertical gradient of the mean tracer abundance, vertical wind transport will naturally produce tracer perturbations on an isobar that are correlated with the vertical velocity field (Fig. 2). For example, if the initial tracer mixing ratio is higher in the lower atmosphere and lower in the upper atmosphere, the upwelling branch of the overturning circulation will transport the higher-mixing-ratio tracers upward and the downwelling branch will transport the lower-mixing-ratio tracers downward from the upper atmosphere. As a result, the tracers on an isobar will be more abundant in the upwelling branch than in the downwelling branch, exhibiting a positive correlation with the vertical velocity field (Fig. 2). After this horizontal tracer distribution is established, the upwelling branch will transport higher-mixing-ratio tracers across an isobar and the downwelling branch will transport lower-mixing-ratio tracers across the same pressure level—the upward and downward tracer fluxes do not cancel out. When averaged over the globe, there will be a net upward tracer flux, resulting an effective upward tracer transport in the global-mean sense.

In the meanwhile, several other processes act to enhance or damp those horizontal tracer perturbations on the isobar. Horizontal mixing/diffusion due to eddies and waves (e.g., breaking of Rossby waves) normally smooth out the tracer variation across the globe. Horizontal advection due to the mean flow may increase or decrease the horizontal tracer variations, depending on the correlation between the horizontal velocity convergence/divergence and the tracer distribution on the isobar. The distribution of tracer sources and sinks due to non-dynamical processes such as chemistry³ also plays an important role. In a simplified picture, those non-dynamical processes could be assumed to relax the tracer distribution back to the chemical equilibrium distribution that the tracers would have in the absence of dynamics, which could be either uniformly distributed across the globe or with a significant variations depending on the local sources and sinks. In principle, quantifying the correlation between the tracer distribution and vertical velocity field is complicated and usually varies case by case. But it is expected that the 1D effective eddy diffusivity K_{eff} depends on the magnitude of the vertical velocity, chemical timescale of the species, horizontal transport timescale and the horizontal variation of the tracer distribution under chemical equilibrium.

³ Hereafter we just use the generic term “chemistry” to represent any non-dynamical processes that affect the tracer distribution, such as chemical reactions in the gas and particle phase, haze and cloud formation, or other phase transition processes.

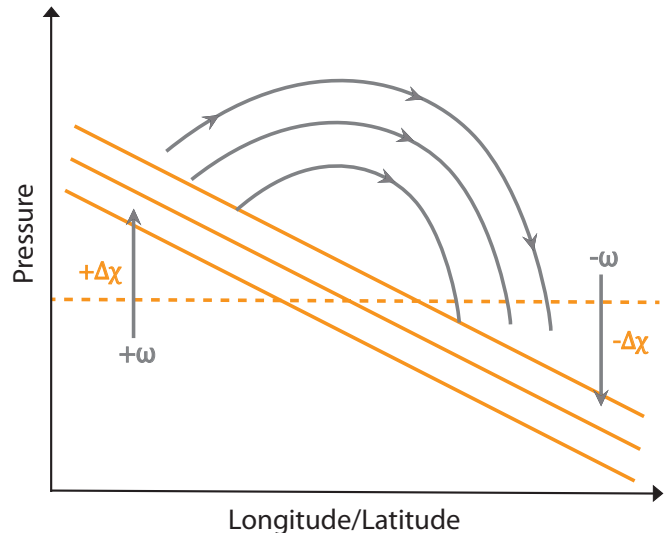


FIG. 2.— Illustration of tracer transport with a large-scale circulation. The orange solid lines indicate constant tracer mixing ratio surfaces. Tracer mixing ratio is higher in the lower atmosphere. Gray lines show horizontal and vertical wind transport with vertical velocity w . $\Delta\chi$ is the deviation of local tracer mixing ratio from the horizontally averaged mixing ratio on an isobar (dashed).

In the Earth regime, Holton (1986) first quantified these effects with a scenario that envisions the vertical mixing is accomplished by a meridional circulation in a 2D (latitude-pressure) framework. The derived eddy diffusivity exhibits a strong dependence on the circulation strength, tracer chemical lifetime and horizontal mixing. Holton showed that the species-dependent eddy diffusivity might help simultaneously explain the vertical profiles of several species in the stratosphere of Earth, whereas the species-independent eddy diffusivity could not. As noted before, the species-independent eddy diffusivity is still widely used in current chemical models for other planets.

In this study we first generalize the 2D theory from Holton (1986) to a 3D atmosphere so that it can be applied to tidally locked exoplanets that are not zonally symmetric as were the fast-rotating planets assumed in Holton’s consideration. We will also analytically formulate K_{eff} using a slightly different approach from Holton (1986) but the physical mechanism is similar. We investigate both the short-lived tracers and long-lived tracers. We also provide 2D and 3D numerical simulations and derived K_{eff} to test our theory, on both fast-rotating planets and tidally locked exoplanets. 2D or 3D numerical tracer transport models have not previously been used to validate analytic theories of K_{eff} ; this study represents the first attempt to do so.

2.2. Governing Equation of Vertical Tracer Transport

Here we develop an approximate analytical theory from first principles to understand the underlying physical mechanisms that govern the global-mean vertical tracer transport in a 3D atmosphere. This theory, in principle, does not assume that the atmosphere needs to be stratified. We include the tracer advection by 3D atmospheric dynamics and tracer chemistry via a simplified chemical scheme to determine how the global-mean tracer transport depends on the general circulation and tracer chemistry. Based on these investigations we will achieve an

analytical parameterization of the 1D effective eddy diffusivity K_{eff} . We will also demarcate different atmospheric regimes in terms of the tracer chemical lifetime and horizontal tracer distribution under chemical equilibrium and validate whether the traditional chemical-diffusion framework is a good approximation in each regime.

First we start from a general 3D tracer transport equation:

$$\frac{D\chi}{Dt} = S \quad (1)$$

where S is the net sources/sinks of the chemical tracer with mixing ratio χ . In principle, isentropic coordinates are more appropriate for discussion of the tracer transport (Andrews et al. 1987). But for simplicity, here we just adopt the log-pressure coordinate $\{x, y, z\}$. The coordinates are defined as $x = a\lambda \sin \phi$ and $y = a\phi$, where a is the planetary radius, λ is longitude and ϕ is latitude. Here, $z \equiv -H \log(p/p_0)$ is the log-pressure where H is a constant reference scale height, p is pressure and p_0 is the pressure at the bottom boundary. $D/Dt = \partial/\partial t + \mathbf{\bar{u}} \cdot \nabla_h + w\partial/\partial z$ is the material derivative. $\nabla_h = (\partial/\partial x, \partial/\partial y)$ is the horizontal gradient at constant pressure. $\mathbf{\bar{u}} = (u, v)$ is the horizontal velocity at constant pressure where u is the zonal (east-west) velocity and v is the meridional (north-south) velocity. $w = Dz/Dt$ is the vertical velocity. In the log-pressure coordinates, Eq. (1) becomes:

$$\frac{\partial\chi}{\partial t} + \mathbf{\bar{u}} \cdot \nabla_h \chi + w \frac{\partial\chi}{\partial z} = S. \quad (2)$$

The continuity equation is:

$$\nabla_h \cdot \mathbf{\bar{u}} + e^{z/H} \frac{\partial}{\partial z} (e^{-z/H} w) = 0. \quad (3)$$

Combining the above two equations, we get the flux form of the tracer-transport equation:

$$\frac{\partial\chi}{\partial t} + \nabla_h \cdot (\chi \mathbf{\bar{u}}) + e^{z/H} \frac{\partial}{\partial z} (e^{-z/H} w \chi) = S. \quad (4)$$

Here we define an eddy-mean decomposition $A = \bar{A} + A'$ where A represents any quantity. \bar{A} is the globally average quantity at constant pressure and A' is the deviation from the mean, or the ‘‘eddy’’ term. Taking the global average of the continuity Eq. (3) to eliminate the horizontal divergence term, we obtain $\bar{w} = 0$ for each atmospheric level if we assume the global-mean vertical velocity \bar{w} vanishes at top and bottom boundaries. Globally averaging Eq. (4) and using $\bar{w} = 0$, we obtain:

$$\frac{\partial\bar{\chi}}{\partial t} + e^{z/H} \frac{\partial}{\partial z} (e^{-z/H} \overline{w\chi'}) = \bar{S}. \quad (5)$$

This is the global-mean vertical tracer transport equation. It states that the evolution of global-mean tracer mixing ratio $\bar{\chi}$ is related to its global-mean vertical eddy fluxes. Based on Eq. (5), $\bar{\chi}$ cannot be solved directly unless we establish a relationship between the mean value and the eddy flux $\overline{w\chi'}$. A conventional assumption is the ‘‘flux-gradient relationship’’ that links the eddy tracer flux to the vertical gradient of the mean value (e.g.

Plumb and Mahlman 1987) by introducing a 1D ‘‘effective eddy diffusion’’ K_{eff} such that:

$$\overline{w\chi'} \approx -K_{eff} \frac{\partial\bar{\chi}}{\partial z}. \quad (6)$$

If Eq. (6) is valid, the global-mean tracer transport equation (5) can be formulated as a vertical diffusion equation:

$$\frac{\partial\bar{\chi}}{\partial t} - e^{z/H} \frac{\partial}{\partial z} (e^{-z/H} K_{eff} \frac{\partial\bar{\chi}}{\partial z}) = \bar{S}. \quad (7)$$

This is the 1D chemical-diffusion equation that is widely used in the field. How to estimate K_{eff} in Eq. (6)? We need to estimate the eddy flux. Subtracting both Eq. (5) and Eq. (3) multiplied by $\bar{\chi}$ from Eq. (4), we obtain:

$$\frac{\partial\chi'}{\partial t} + \nabla_h \cdot (\chi' \mathbf{\bar{u}}) + w \frac{\partial\chi'}{\partial z} + e^{z/H} \frac{\partial}{\partial z} [e^{-z/H} (w\chi' - \overline{w\chi'})] = S'. \quad (8)$$

Now we need to estimate the horizontal tracer variation χ' along an isobar. Here we discuss two situations in terms of the tracer chemical lifetime: (1) a short-lived tracer with a chemical timescale smaller than the dynamical timescale and (2) a long-lived tracer, or a ‘‘quasi-conservative’’ tracer, with a significantly longer chemical lifetime than the dynamical timescale.

2.3. Short-lived Tracers

In this situation, we can estimate χ' from the vertical gradient of $\bar{\chi}$ under following four assumptions.

(i) We neglect the temporal variation (time evolution) of the χ' in statistical steady state. The first term on the left hand side of Eq. (8) can be neglected.

(ii) We assume the complicated eddy term (the last term in the left hand side of Eq. (8)) is much smaller than the third term and thus can be neglected. In other words, the deviation of the eddy flux from its global mean is smaller than the local vertical transport of the vertical gradient of the global-mean tracer, for example, in the case where the deviation of the tracer mixing ratio from the mean is small and the material surface is not significantly distorted (χ' is small), or that the vertical gradient of χ' is small compared with the mean tracer gradient.

(iii) We approximate the horizontal tracer eddy flux term $\nabla_h \cdot (\chi' \mathbf{\bar{u}}) \approx \chi'/\tau_d$ where τ_d is the characteristic dynamical timescale in the horizontal mixing processes. In general, under different situations, this divergence term could act in an advective way, or in a diffusive way, motivating two possible ways of formulating the dynamical timescale. In the advection, the dynamical transport timescale $\tau_d \approx L_h/U_{adv}$ where L_h is horizontal characteristic length scale (usually taken as the planetary radius a), U_{adv} is the horizontal wind speed. In the diffusive case, the dynamical timescale $\tau_d \approx L_h^2/D$ where D is the effective horizontal eddy diffusivity. Note that in this linear relaxation approximation, we have assumed that horizontal dynamics always reduces the horizontal variation of the tracer. This is generally holds true if the horizontal tracer field is not complicated. Some exceptions will be discussed in the numerical simulation sections later.

(iv) For simplicity, we consider a linear chemical scheme which relaxes the tracer distribution towards lo-

cal chemical equilibrium χ_0 in a timescale τ_c :

$$S = \frac{\chi_0 - \chi}{\tau_c}. \quad (9)$$

If chemical equilibrium tracer distribution is assumed to be uniformly distributed across the globe, χ_0 is constant along an isobar and only a function of pressure, for example, the species advected upward from the deep atmosphere with a uniform thermochemical source. In general, the equilibrium chemical tracer abundance depends on many local factors, such as temperature, abundances of other species, photon fluxes and precipitating ion fluxes. It is expected that photochemical species will exhibit χ_0 that varies between the equator and poles. These effects might have more pronounced influences on the horizontal distributions of χ_0 on tidally locked exoplanets than on solar system planets. Without losing generality, here we consider a non-uniform horizontal distribution of the chemical equilibrium: $\chi_0 = \bar{\chi}_0 + \chi'_0$, where $\bar{\chi}_0$ is the global-mean of χ_0 which is only a function of pressure, and χ'_0 is the departure of equilibrium tracer abundance from its global mean. Inserting χ_0 into Eq. (9), we obtain the globally averaged chemical source/sink term $\bar{S} = (\bar{\chi}_0 - \bar{\chi})/\tau_c$ and the departure $S' = (\chi'_0 - \chi')/\tau_c$.

With the above assumptions, Eq. (8) can be written:

$$w \frac{\partial \bar{\chi}}{\partial z} + \frac{\chi'}{\tau_d} = \frac{\chi'_0 - \chi'}{\tau_c}. \quad (10)$$

We solve for χ' :

$$\chi' = \frac{-w \frac{\partial \bar{\chi}}{\partial z} + \tau_c^{-1} \chi'_0}{\tau_d^{-1} + \tau_c^{-1}}. \quad (11)$$

This expression for the 3D distribution of χ' is qualitatively similar to the previous 2D model result in Holton (1986) with a photochemical source (c.f., his Eq. 19). However, Holton (1986) mainly focused on a special case ($\chi'_0 = 0$) without further elaborating the physical meaning of the general expression Eq. (11). Here we explicitly point out that the global-mean vertical tracer transport is composed of two physical processes: a diffusion process and a non-diffusive process. Based on Eq. (11), the global-mean vertical tracer flux $\overline{w\chi'}$ is:

$$\overline{w\chi'} = \frac{-\overline{w^2}}{\tau_d^{-1} + \tau_c^{-1}} \frac{\partial \bar{\chi}}{\partial z} + \frac{\overline{w\chi'_0}}{1 + \tau_d^{-1}\tau_c}. \quad (12)$$

The first term in Eq. (12) implies diffusive behavior, because this term's contribution to the tracer vertical flux is proportional to the vertical gradient of the mean tracer abundance. But the second term does not depend on the mean tracer gradient, suggesting a non-diffusive behavior. Instead, the second term originates from the correlation between the equilibrium tracer distribution and the vertical wind field. It can be neglected if the tracer under chemical equilibrium is more or less uniformly distributed across the globe. However, if the equilibrium tracer distribution is significantly non-uniform (for instance, if, in chemical equilibrium, the equator and poles have strongly differing chemical abundances), the conventional ‘‘eddy diffusion’’ framework breaks down because the non-diffusive process might dominate the vertical tracer transport in the global-mean sense. To

elaborate the physics here, we now further discuss these two cases: a uniformly distributed tracer under chemical equilibrium and a non-uniform case.

2.3.1. Tracer with Uniform Chemical Equilibrium: Diffusive case

If the equilibrium tracer distribution is uniformly distributed (i.e., $\chi'_0 = 0$), the non-diffusive term in Eq. (12) vanishes. In this special case of short chemical lifetime (among other assumptions), mean tracer transport can be regarded as a diffusive process and the eddy diffusivity K_{eff} can be parameterized based on the relationship between eddy tracer flux to the global-mean tracer gradient based on Eq. (12) and Eq. (6):

$$K_{eff} \approx \frac{\overline{w^2}}{\tau_d^{-1} + \tau_c^{-1}}. \quad (13)$$

This result is also consistent with that from a zonal-mean 2D model in Holton (1986) with a uniform chemical equilibrium abundance. The parameterized K_{eff} depends on circulation strength, chemical lifetime of the tracer and horizontal transport/mixing timescale in the atmosphere. It is expected that different chemical tracers are subjected to different eddy diffusivity strength, which has not been considered to date in 1D chemical models of planetary atmospheres.

If $\chi'_0 = 0$, the horizontal distribution of χ' , deviation of the tracer mixing ratio from the mean on an isobar, is correlated with the horizontal distribution of vertical velocity w at the same pressure level (Eq. 11):

$$\chi' = \frac{-w \frac{\partial \bar{\chi}}{\partial z}}{\tau_d^{-1} + \tau_c^{-1}}. \quad (14)$$

If the tracer is diffused upward with a uniform chemical equilibrium abundance in the deep atmosphere but is photochemically destroyed in the upper atmosphere—for example, sulfur dioxide on Venus, methane on Jupiter or water on hot Jupiters—the mean tracer gradient $\partial \bar{\chi}/\partial z$ is negative, and therefore χ' is positively correlated with w . In other words, the tracer mixing ratio is higher in the upward wind region and lower in the downwelling region. This correlation implies that the circulation transports higher mixing ratio tracer upward and transports lower mixing ratio tracer downward (Fig. 2). The net effect is a net upward transport of the tracer, the magnitude of which can be quantified by K_{eff} .

On the other hand, if the tracer source is in the upper atmosphere, for example, chemically produced species which are uniformly distributed under chemical equilibrium, or oxygen species with uniform fluxes from comets into the upper atmospheres of giant planets (Moses & Poppe 2017), the eddy diffusivity in the region below the source could be discussed in a similar way. In this case, the mean tracer gradient $\partial \bar{\chi}/\partial z$ is generally positive. Eq. (13) predicts that χ' is anti-correlated with w , i.e. the tracer has a higher mixing ratio in the downwelling region and a lower mixing ratio in the upwelling region. This anti-correlation pattern implies a net downward transport of the tracer. In summary, the eddy diffusivity K_{eff} introduced here will always transport the tracer away from its source region.

If the circulation is stronger, i.e., w is larger, the horizontal variation of the tracer mixing ratio will be larger. If the chemical loss or the horizontal mixing due to advection or diffusion is stronger, i.e., τ_d and τ_c are smaller, the tracer variation is smaller. As a result, a large-scale circulation enhances the tracer variation, whereas chemical relaxation and horizontal tracer mixing homogenizes the tracer distribution across the isobar. The tracer distribution reaches equilibrium when the two competing processes balance each other. The resulting eddy diffusivity is larger if the circulation is stronger, the tracer chemical lifetime is longer, or the horizontal mixing timescale is longer.

To further elaborate how K_{eff} depends on the chemical lifetime τ_c , we consider two different tracers, one with short τ_c and another with long τ_c , that both exist in an atmosphere with a specified 3D atmospheric circulation. For concreteness, imagine that the background tracer abundance of both tracers decreases upward, with the same background gradient for both tracers. Because of the advection, for both tracers, the tracer abundance on an isobar will be greater in upwelling regions and smaller in downwelling regions, implying an upward flux of the tracer in both cases. However, when τ_c is short, the chemistry very strongly relaxes the abundance toward equilibrium, whereas with long τ_c , this relaxation is weak. This implies that, in statistical equilibrium, the deviation of the actual tracer abundance from chemical equilibrium, χ' , is greater when τ_c is long than when it is short. Since the circulation is the same in the two cases, the upward tracer flux $\overline{w\chi'}$ is greater when τ_c is long and smaller when τ_c is short. Given the definition of eddy diffusivity $K_{eff} = -\overline{w\chi'}/\frac{\partial\overline{\chi}}{\partial z}$ from Eq. (6), we thus have the situation where the tracer with short τ_c has a smaller K_{eff} than the tracer with large τ_c —even though the atmospheric circulation, by definition, is precisely the same for the two tracers. Indeed, for this simple situation, the value of K_{eff} would go to zero in the limit $\tau_c \rightarrow 0$, because in that case, the tracer is constant on isobars, so there is no net correlation between vertical velocity and tracer abundance, implying that the upward flux of tracer is zero.

2.3.2. Tracer with Non-uniform Chemical Equilibrium: Non-diffusive Component

The horizontal distribution of tracer equilibrium abundance could be significantly non-uniform, i.e., $\chi'_0 \neq 0$. This could occur if there is a local plume source of the species at surface, such as volcanic eruption. A more common case is photochemically produced species like ozone on terrestrial planets or ethane on giant planets, where the incoming ultraviolet solar flux changes with the solar angle, leading to different photochemical equilibrium abundances at different latitudes. An extreme example is the tidally locked exoplanets, on which different chemical equilibrium states are expected between the permanent dayside and nightside for a tracer whose chemistry critically depends on factors such as temperature, incoming photon and ion fluxes. For example, formation of condensed haze/cloud particles favor the colder nightside than the warmer dayside. For another example, species produced by photochemistry or ion chemistry are expected to have a larger equilibrium abundance on the dayside than on the nightside.

In these situations, the dependence of K_{eff} on the circulation and tracer chemistry is more complicated. The eddy tracer flux due to the non-diffusive process, i.e., the second term in the right hand side of Eq. (12), cannot be neglected. The horizontal distribution of χ' might not be strongly correlated with the horizontal distribution of vertical velocity w at the same pressure level (Eq. 11). The correlation term between the non-uniform chemical equilibrium abundance and vertical velocity $\overline{w\chi'_0}$ could have a significant effect on K_{eff} (Eq. 12). Physically speaking, in the case with uniform chemical equilibrium abundance, atmosphere circulation will shape the initially homogeneous tracer distribution toward a correlation between w and χ' that has the opposite sign as the background gradient; in other words, it causes $\overline{w\chi'}$ to have opposite sign as $\partial\overline{\chi}/\partial z$, which in turn implies that the tracer is mixed down the vertical gradient of the horizontal-mean tracer abundance. In the case of non-uniform chemical equilibrium case, the background of the tracer distribution under chemical equilibrium might correlate or anti-correlate with the vertical velocity pattern, causing an additional or even dominant contribution to the net vertical tracer transport flux in an essentially non-diffusive way. Whether this contribution will enhance or reduce the net vertical mixing efficiency depends on the correlation as well as the vertical gradient of the mean tracer (Eq. 12).

If we still adopt the traditional “eddy diffusion” framework, one might try to put a correction term in Eq. (13) to approximate the non-diffusive behavior and estimate K_{eff} for the tracers with non-uniform chemical equilibrium:

$$K_{eff} \approx \frac{\overline{w^2}}{\tau_d^{-1} + \tau_c^{-1}} - \frac{\overline{w\chi'_0}}{1 + \tau_d^{-1}\tau_c} \left(\frac{\partial\overline{\chi}}{\partial z}\right)^{-1}. \quad (15)$$

The second term on the right hand side represents the first-order correction which might be useful if the non-diffusive contribution is not large. Eq. (15) is no longer a first-principle estimate of K_{eff} because it depends on the vertical gradient of the global-mean tracer mixing ratio, a quantity that requires K_{eff} to solve for. One could imagine an iterative process between the chemical-diffusion simulation and updating K_{eff} might lead to a final steady state of the system. Nevertheless, it must be borne in mind that describing the mixing with an eddy diffusivity is rather misleading in this situation, because the tracer flux is not proportional to the tracer gradient (as it would be in a true diffusive problem) and the governing equation is not diffusive.

We emphasize that the K_{eff} expression with the non-diffusive correction needs to be used cautiously in 1D chemical-diffusion simulations and can only be used when the non-diffusive contribution is not dominant. If the second term dominates and is negative, the predicted K_{eff} can be negative in some situation. For example, if the tracer lifetime is very short, $\tau_c \rightarrow 0$, Eq. (15) becomes:

$$K_{eff} \approx -\overline{w\chi'_0} \left(\frac{\partial\overline{\chi}}{\partial z}\right)^{-1} \quad (16)$$

In this limit, the diffusive term vanishes and the non-diffusive term dominates. Vertical tracer mixing is significantly controlled by the correlation between the chemical equilibrium distribution and the vertical velocity dis-

tribution. If the correlation is positive, i.e., tracer is more abundant in the upwelling region than the downwelling region due to chemistry, and if the tracer is produced at the top, i.e., the vertical gradient of the mean tracer mixing ratio is positive, the derived K_{eff} is negative (Eq. 16). A negative effective eddy diffusivity does not make sense physically as it suggests the tracer is mixed towards its source. The reason is simply because the global-mean vertical tracer transport is essentially non-diffusive in this case.

For a given vertical gradient of global-mean tracer, K_{eff} becomes larger if the circulation is stronger, the tracer chemical lifetime is longer, and the horizontal mixing timescale is longer. This trend is consistent with that in the case with uniform chemical equilibrium abundance. Interestingly, as the chemical timescale becomes longer, the diffusive term gets larger and the non-diffusive term becomes smaller, perhaps because the longer-lived tracers are more controlled by the dynamical transport so that the non-uniform chemical equilibrium has less effect. Thus the non-diffusive correction in Eq. (15) should work better for species with relatively long timescales.

2.4. Long-lived Tracers

If the tracer chemical lifetime is long and the tracer is almost inert, the material surfaces (tracer contours) are usually distorted significantly⁴. The above discussion for short-lived tracers could be violated since the assumption (ii) in Section 2.1.1 might no longer be valid. It is expected that the 3D distribution of such a “quasi-conservative” tracer is significantly controlled the atmospheric dynamics. Due to the complicated dynamical transport behavior, no simple analytical theory of the global-mean vertical tracer transport exists, and thus the corresponding K_{eff} is not generally known.

Although it is expected that there are some non-diffusive effects in this regime, the diffusive framework may still be useful. If we still apply the K_{eff} theory in Section 2.3 to this regime and let $\tau_c \rightarrow \infty$, the non-diffusive contribution vanishes (Eq. 12). In this case, the influence of the chemical equilibrium tracer distribution is negligible and Eq. (15) is reduced to Eq. (13). One might expect K_{eff} to approach its asymptotic value in Eq. (13):

$$K_{eff} \approx \overline{w^2} \tau_d = \hat{w} L_v \quad (17)$$

where we have introduced a vertical transport length scale $L_v = \hat{w} \tau_d$ and \hat{w} is the root-mean-square of the vertical velocity $\hat{w} = (\overline{w^2})^{1/2}$. Here the vertical transport timescale is assumed as the horizontal tracer mixing timescale τ_d due to the continuity equation. Eq. (17) is in the similar form of that from the mixing length theory although there is no convective or small-scale mixing due to wave breaking in our theory. Using L_v , the effective eddy diffusivity (Eq. 13) for short-lived tracers with

uniform chemical equilibrium (Section 2.3.1) can also be represented as:

$$K_{eff} = \frac{\hat{w} L_v}{1 + \tau_d \tau_c^{-1}}. \quad (18)$$

The magnitude of the change in K_{eff} depends on the ratio of the timescales between the dynamical and chemical processes: τ_d/τ_c . In the long-lived tracer regime where $\tau_c \rightarrow \infty$, the effective eddy diffusivity K_{eff} approaches Eq. (17).

The vertical transport length scale L_v in our K_{eff} theory cannot be arbitrarily chosen. It critically depends on the atmospheric dynamics, specifically the vertical velocity \hat{w} and the horizontal dynamical timescale τ_d . If the dynamical timescale τ_d for horizontal tracer mixing is equal to the global horizontal advection timescale a/U where a is approximately the planetary radius, through continuity τ_d should be approximately H/\hat{w} . Then L_v would be equal to the pressure scale height H . If the horizontal mixing timescale is longer (or shorter) than the horizontal advection timescale, L_v is then larger (or smaller) than H by that same factor. Using the vertical velocity from general circulation models and simply assuming L_v is H , some previous models (e.g., Lewis et al. 2010, Moses et al. 2011) estimated the eddy diffusivities on exoplanets based on Eq. (17). Those estimates were much larger than the eddy diffusivity derived based on 3D passive tracer simulations (Parmentier et al. 2013).

There are two reasons. First, K_{eff} estimated from Eq. (17) is the maximum eddy diffusivity one can obtain from Eq. (18). For short-lived tracers, the effective eddy diffusivity should be smaller than that from Eq. (17). Second, in the long-lived tracer regime, tracers are significantly controlled by atmospheric dynamics and the horizontal dynamical timescale τ_d might be different from the global horizontal advection timescale a/U . Thus the vertical characteristic transport length scale L_v in Eq. (17) and (18) could be different from H . This has also been noted in the studies of tracer transport in the convective atmospheres. For example, Smith (1998) investigated dynamical quenching of chemical tracers in convective atmospheres and found that vertical transport length scale in the traditional mixing length theory should depend on the chemical tracer equilibrium distribution as well as the chemical and dynamical timescales. Recent work by Bordwell et al. (2018) explored the chemical tracer transport using non-rotating local convective box models. They found that using the chemical scale height as the vertical transport length scale, which is usually smaller than the scale height H , leads to a better prediction of the chemical quenching levels.

We reiterate that the assumptions used to derive Eq. (17) likely break down in the regime of long-lived tracers, so it may be that the qualitative dependencies implied in Eq. (17) are not rigorously accurate when the tracers are long-lived. In our theory we have dropped the last term in the left hand side in Eq. (8), which might become important in the long-lived regime. As we will demonstrate in the numerical simulations later, this non-linear eddy term could potentially enhance or decrease the global tracer mixing efficiency. We also emphasize that, although we adopt the diffusive framework here in the long-lived tracer regime, the tracer transport in this

⁴ If the tracer is absolutely inert with a very long lifetime, it will be completely homogenized over the globe by the horizontal transport. But in this study we do not investigate this type of real conservative, well-mixed tracers. The “long-lived tracer” in our study stands for the species with a significantly long chemical lifetime so that the atmospheric dynamics greatly shapes its material surface, but the horizontal variation of the tracer distribution is still not small.

regime may not always behave diffusively. As we will also show later in the numerical simulations, the diffusive assumption could break down in some cases when the tracer material surface is distorted significantly and non-diffusive effects are substantial.

In sum, in this section we have developed an approximate analytical theory for the 1D global-mean tracer transport in a 3D atmosphere. We demarcated three atmospheric regimes in terms of the tracer chemical lifetime and horizontal tracer distribution under chemical equilibrium: (I) a short-lived tracer with chemical equilibrium abundance uniformly distributed across the globe, (II) a short-lived tracer with a non-uniform distribution of the chemical equilibrium abundance, and (III) a long-lived tracer regime with the tracer material surface significantly controlled by dynamics. The underlying physical mechanisms governing the global-mean vertical tracer transport in the three regimes are different. The traditional chemical-diffusion assumption is mostly valid in the first regime but could be violated in the second and third regimes. We predicted the analytical expression of the 1D effective eddy diffusivity K_{eff} for the global-mean vertical tracer transport. K_{eff} depends on both atmospheric dynamics and tracer chemistry. Crudely speaking, if the atmospheric dynamics is fixed, K_{eff} roughly scales with the tracer chemical lifetime $K_{eff} \propto \tau_c$ (Eq. 13) when the tracer lifetime is short (regime I) and approaches to a constant value when the tracer lifetime is long (regime III, Eq. 17). We also found that in the short-lived tracer regime (regime I), K_{eff} roughly scales with the vertical velocity square $K_{eff} \propto \hat{w}^2$ (Eq. 13), but in the long-lived tracer regime (regime III), it scales with root-mean-square of the vertical velocity $K_{eff} \propto \hat{w}$ (Eq. 17). Next, we will perform a series of numerical experiments to quantitatively verify our theoretical arguments. We will primarily focus on stratified atmospheres here.

3. NUMERICAL SIMULATIONS

In our numerical simulations, we will only study passive tracers, i.e., no radiative feedback from the tracer to the dynamics. First, we consider a fast-rotating planet on which the tracer is uniformly distributed with longitude. Most of the planetary atmospheres in the solar system are close to this regime. This is essentially a 2D tracer transport problem that can be studied using a 2D zonally symmetric model. Then we investigate the tracer transport on a tidally locked planet using 3D general circulation models and explore the behaviors of tracers with both uniform and non-uniform chemical equilibrium situations.

3.1. 2D Simulation with Meridional Circulation

2D zonal-mean tracer transport has been extensively discussed in the Earth literature (e.g., Holton 1986). But till now there has not been a thorough and specific study on the global-mean eddy diffusivity using 2D numerical simulations with chemical tracers. On a fast-rotating planet, when averaged zonally, the meridional circulation that transports the tracer (like the one shown in Fig. 2) should be considered as the ‘‘Lagrangian mean circulation’’, which can be approximated by a Transformed Eulerian Mean (TEM) circulation (Andrews & McIntyre

1976), and called the ‘‘residual mean circulation’’. Another formalism of the zonal-mean tracer transport introduced by Plumb & Mahlman (1987) used the ‘‘effective transport velocity’’. The difference between the two circulation formalisms is usually small in Earth’s stratosphere and vanishes if the waves are linear, steady, and adiabatic (Andrews et al. 1987).

In both frameworks, the zonal-mean eddy tracer fluxes can be parameterized as diffusive fluxes using a symmetric ‘‘diffusion tensor’’ with four parameters (diffusivities): K_{yy} , K_{zz} , K_{yz} and K_{zy} (Andrews et al. 1987). K_{yz} and K_{zy} are negligible in isentropic coordinates (Tung 1982). As here we mainly focus on the stratified atmosphere where the inclination between the isobars and isentropes is usually small, we can ignore K_{yz} and K_{zy} in 2D chemical tracer transport simulations in this study (e.g., Garcia & Solomon 1983, Shia et al. 1989).

A 3D model would naturally produce small-scale eddies that would cause mixing, and if the eddies were fully resolved, no parameterization of diffusive fluxes is needed in the tracer transport. But in our 2D framework that ignores any role for such eddies, even for a planet with a great degree of zonal symmetry at large scales (like Earth or Jupiter), we have to parameterize the horizontal and vertical diffusivities K_{yy} and K_{zz} as a separately included process. In principle K_{yy} and K_{zz} can be estimated from the Eliassen-Palm flux (Andrews et al. 1987) in a 3D model. But for our purpose of studying the response of the chemical tracer distribution to the dynamics and the global-mean vertical tracer mixing, we just prescribe the diffusivities and the circulation.

The governing equation of a 2D chemical transport system using the coordinates of log-pressure and latitude, can be written as (Shia et al. 1989, Shia et al. 1990, Zhang et al. 2013b):

$$\frac{\partial \chi}{\partial t} + v^* \frac{\partial \chi}{\partial y} + w^* \frac{\partial \chi}{\partial z} - \frac{1}{\cos \phi} \frac{\partial}{\partial y} (\cos \phi K_{yy} \frac{\partial \chi}{\partial y}) - e^{-z/H} \frac{\partial}{\partial z} (e^{-z/H} K_{zz} \frac{\partial \chi}{\partial z}) = S \quad (19)$$

where $\phi = y/a$ is latitude and a is the planetary radius. H is the pressure scale height. Residual circulation velocities are v^* and w^* in the meridional and vertical directions, respectively. For a 2D circulation pattern, we can introduce a mass streamfunction ψ such that:

$$v^* = -\frac{1}{2\pi a \rho_0 \cos \phi} e^{z/H} \frac{\partial}{\partial z} (e^{-z/H} \psi) \quad (20a)$$

$$w^* = \frac{1}{2\pi a \rho_0 \cos \phi} \frac{\partial \psi}{\partial y} \quad (20b)$$

where ρ_0 is the reference density of the atmosphere at log-pressure $z = 0$. With prescribed distributions of ψ , K_{yy} and K_{zz} , we solve the governing equations using the Caltech/JPL 2D kinetics model (for numerics, refer to Shia et al. 1990). We use the Prather scheme for the 2D tracer advection (Prather 1986). The model has been rigorously tested against multiple exact solutions under various conditions (Shia et al. 1990, Zhang et al. 2013b).

We adopted two different meridional circulation patterns (see Section 4 in Zhang et al. 2013b). The circulation ψ_A is an equator-to-pole pattern and circulation ψ_B is pole-to-pole, corresponding to planets with low obliquity.

TABLE 1
2D SIMULATION CASES IN THIS STUDY.

Experiment	Streamfunction	K_{yy} ($\text{m}^2 \text{s}^{-1}$)	Tracer
I	ψ_A	10	Deep source
II	ψ_B	10	Deep source
III	ψ_A	10	Top source
IV	ψ_A	10^6	Deep source

uity and high obliquity, respectively:

$$\psi_A = 2\pi a^2 \rho_0 w_0 e^{\eta z/H} \sin \phi \cos^2 \phi \quad (21a)$$

$$\psi_B = 2\pi a^2 \rho_0 w_0 e^{\eta z/H} \cos^2 \phi. \quad (21b)$$

The mass streamfunctions and vertical velocities of the two circulation patterns are shown in Fig. 3. For both circulations, the area-weighted global-mean vertical velocity scale is about $\gamma w_0 e^{\eta z/H}$ where γ is an order-unity pre-factor originating from the global average.⁵

For a fast-rotating planet, we assume that the tracer chemical equilibrium is uniform with latitude, at least compared with possibly large day-night contrast on tidally-locked planets that we will discuss later. In this 2D chemical-advective-diffusive system, both the meridional advection and horizontal eddy diffusion contribute to the horizontal tracer mixing, and both the vertical advection and vertical eddy diffusion contribute to the vertical tracer transport. The 1D effective eddy diffusivity K_{eff} in this system can be analytically predicted following the procedure introduced in Section 2. But since here we have to treat explicitly the eddy diffusion terms K_{yy} and K_{zz} originating from zonal-mean 2D dynamics, we provided a detailed derivation of K_{eff} in this 2D system in the Appendix. We show that the vertical eddy diffusion by K_{zz} in Eq. (19) can be treated as an additive term in the global-mean effective eddy diffusivity K_{eff} . The K_{eff} for the uniform-chemical-equilibrium situation in the 2D framework can be expressed as:

$$K_{eff} \approx K_{zz} + \frac{\gamma^2 w_0^2 e^{2\eta z/H}}{K_{yy} a^{-2} + \gamma w_0 e^{\eta z/H} H^{-1} + \tau_c^{-1}}. \quad (22)$$

In the second term on the right hand side, the three terms in the denominator correspond to horizontal tracer diffusion due to eddies and waves, horizontal tracer advection by zonal-mean flow and tracer chemistry, respectively. Here we have assumed the horizontal transport length scale $L_h \sim a$ and vertical transport length scale $L_v \sim H$. See Appendix for more details.

We use Jupiter’s parameters in these 2D simulations but with an isothermal atmosphere of 150 K from 3000 Pa to about 0.2 Pa for simplicity. For the circulation patterns, we adopt $w_0 = 10^{-5} \text{ m s}^{-1}$ and $\eta = 0.5$. Given a pressure scale height H of about 25 km, the vertical advection timescale changes from 10^9 s at the bottom to about 10^7 s at the top. The vertical profile of the advection timescale is similar to the empirical vertical mixing timescale derived from H^2/K_z where K_z is the empirical eddy diffusivity in the 1D stratospheric chemical model on Jupiter (Moses et al. 2005, also see Fig. 1). The hori-

zonal advection timescale in our model is about 10^8 s at 100 Pa, comparable to the vertical circulation timescale due to the continuity constraint. This horizontal transport timescale is also similar to that inferred from Voyager and Cassini observations (Nixon et al. 2010, Zhang et al. 2013a).

We designed four 2D experiments (Table 1) and simulated 9 tracers in each experiment. The vertical profile of equilibrium tracer mixing ratio χ_{eq} is assumed to be a power-law function of pressure $\chi_{eq}(p) = 10^{-5}(p/p_0)^{1.7}$ where $p_0 = 3000$ Pa is the pressure at the bottom boundary. χ_{eq} starts from 10^{-5} at bottom and decreases towards 10^{-12} at the top of the atmosphere. A linear chemical scheme (Eq. 9) is applied to each tracer with a relaxation timescale τ_c that varies from 10^7 to 10^{11} s. The chemical timescale of the i th tracer is assumed as $\tau_c = 10^{6.5+0.5i}$ s. We also tested different horizontal diffusional coefficients K_{yy} . In all cases, we set the vertical diffusion coefficients K_{zz} zero because here we mainly investigate the influence of the large-scale overturning circulation, horizontal mixing and chemical source/sink on the global-mean vertical tracer transport in this study. According to Eq. (22), the influence of K_{zz} in the 2D simulation is trivial because it can just be treated as an additive term in K_{eff} .

We discretized the atmosphere into 35 latitudes in the horizontal dimension, corresponding to 5° per grid cell. Vertically, the log-pressure grid is evenly spaced in 80 layers from 3000 Pa to about 0.2 Pa. The time step in the simulations is 10^5 second. We ran the simulations for about 10^{13} s to ensure the spatial distributions of the tracers have reached the steady state. The tracer abundances were averaged over the last 10^9 s for analysis.

Experiment I (Fig. 3) is the standard case with an equator-to-pole streamfunction ψ_A and a constant horizontal eddy diffusivity $K_{yy} = 10 \text{ m}^2 \text{ s}^{-1}$. This is a “deep source” case in which tracer is advected upward from the deep atmosphere. Experiment II is same as Experiment I but with a different circulation pattern ψ_B . Experiment III is also same as Experiment I but with a “top chemical source”. The equilibrium tracer mixing ratio, while still uniform across the latitude, is large at top (10^{-5}) and small at the bottom (10^{-12}). In Experiments I to III, the horizontal eddy diffusion timescale is $a^2/K_{yy} \sim 5 \times 10^{14}$ s. The diffusive transport is much less efficient compared with the horizontal advection and can be neglected (timescale of $10^7 - 10^9$ s). We designed Experiment IV using the streamfunction ψ_A but horizontal eddy diffusivity K_{yy} enhanced to $10^6 \text{ m}^2 \text{ s}^{-1}$. In this case, the diffusive timescale is about 5×10^9 s, comparable to the circulation timescale (but the K_{zz} is still zero). In this setup we can test the influence of the horizontal eddy mixing to the global-mean vertical tracer transport.

The steady state results in Experiments I and II are

⁵ γ is $2/\sqrt{5}$ for ψ_A and $2/\sqrt{3}$ for ψ_B from the global integrations of Eq. (21a) and (21b), respectively. Thus the effective transport is a bit stronger using the circulation pattern B.

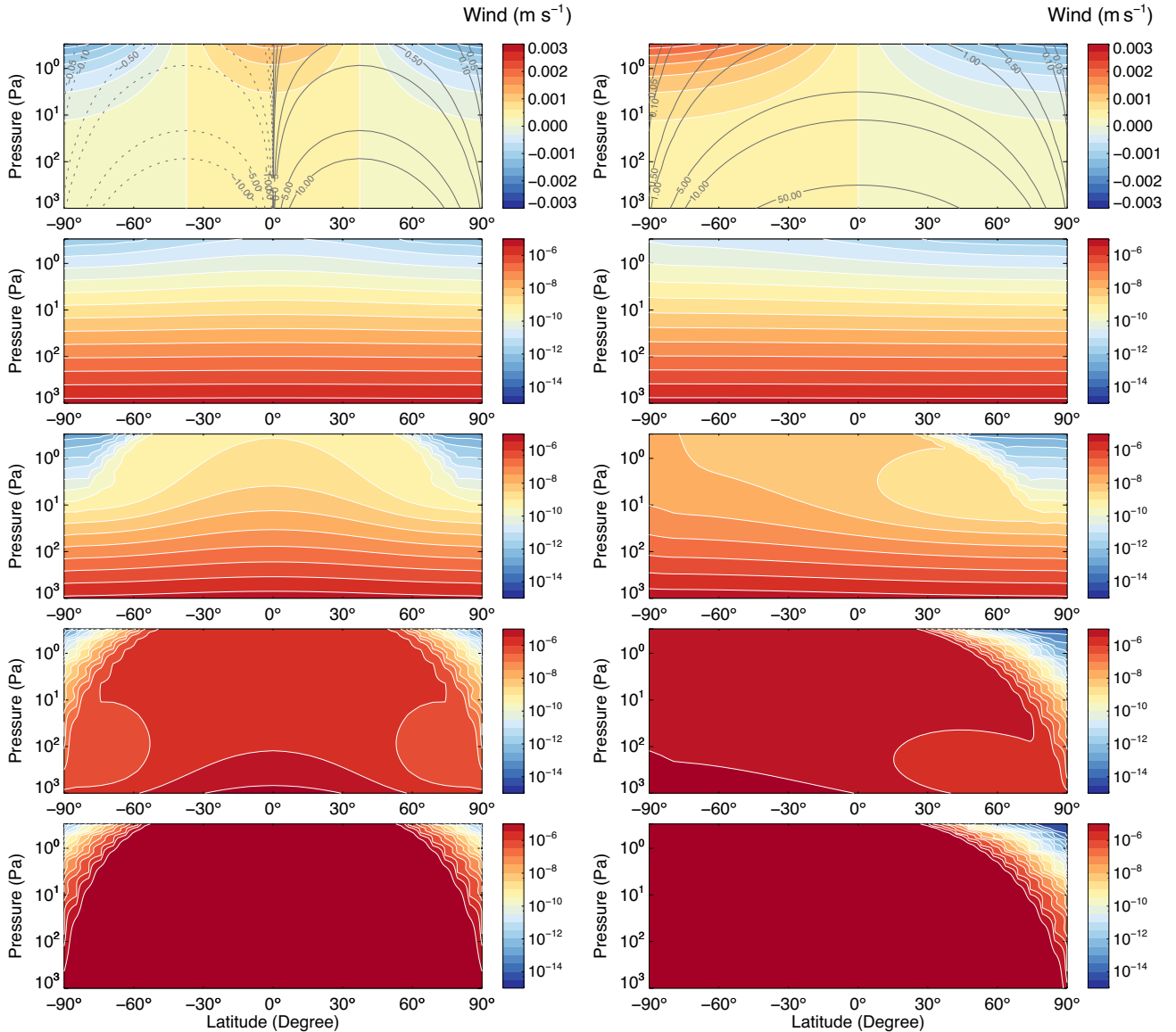


FIG. 3.— Latitude-pressure maps of experiments I (left) and II (right). First row: vertical winds (color) and mass streamfunctions (contours, in units of $10^{13} \text{ Kg s}^{-1}$). Starting from the second row we show volume mixing ratio maps of tracers with chemical timescales of 10^7 s , 10^8 s , 10^9 s and 10^{10} s from top to the bottom, respectively.

shown in Fig. 3. Although the final tracer distributions are different between the two experiments due to different circulation patterns, some common behaviors exist. The short-lived tracers are uniformly distributed across latitude. As the tracer chemical lifetime increases, the effect of the circulation becomes stronger. In the upwelling region, higher-mixing-ratio tracers are transported upward from their deep source; while in the downwelling region, lower-mixing-ratio tracers are transported from the upper atmosphere. As a result, the tracer mixing ratio is higher in the upwelling region and lower in the downwelling region on an isobar. The final latitudinal variations of the short-lived tracers follow the pattern of the vertical velocity (Fig. 3 and Eq. 14). However, if the tracer chemical timescale is very long (Fig. 3, bottom row), the tracers tend to be homogenized by the circulations.

We numerically derive K_{eff} based on the simulation results and the flux-gradient relationship (Eq. 6) and

compare with the analytical prediction (Eq. 22). First, we averaged the tracer distributions with latitude in an area-weighted-mean fashion. The vertical profiles of the global-mean tracer mixing ratios are shown in Fig. 4 for Experiment I and Fig. 5 for Experiment II, respectively. The vertical profiles of short-lived tracers are close to the chemical equilibrium profile but that of the long-lived tracers are almost well mixed and “quench” to the lower atmosphere values because the global circulations efficiently smooth out their vertical gradients. We then derived the 1D effective eddy diffusivity K_{eff} by equating the eddy diffusive flux to the global-mean net vertical flux of the tracers (Eq. 6, Fig. 4 and Fig. 5). Our analytical prediction based on Eq. (22) matches the numerical results well.

K_{eff} increases from the bottom towards the top of the atmosphere because the vertical velocity is larger and transport is stronger in the upper atmosphere. Our theory predicts that K_{eff} roughly scales with the square of

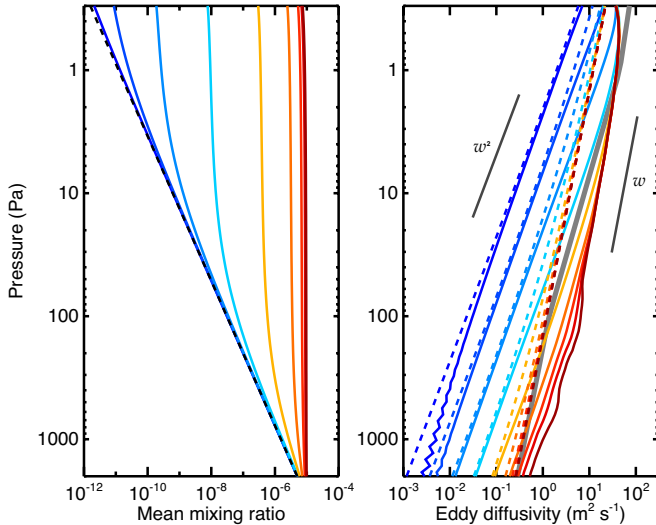


FIG. 4.— Vertical profiles of the global-mean volume mixing ratio (left) and derived effective eddy diffusivity (right) from Experiment I. Different colors from cold (blue) to warm (red) represent tracers with different chemical timescales from short to long, ranging from 10^7 s to 10^{11} s. The prescribed equilibrium tracer mixing ratio profile is shown in the dashed line in the left panel. The predicted eddy diffusivity profiles based on Eq. (22) are shown in dashed in the right panel. The solid lines are derived from the simulations. The thick gray line indicates the empirical eddy diffusivity profile used in current photochemical models in Jupiter’s stratosphere (Moses et al. 2005, Moses & Poppe 2017).

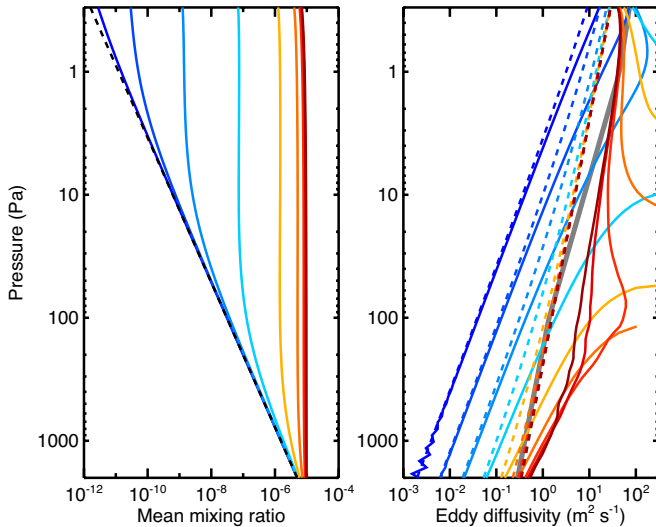


FIG. 5.— Same as Fig. 4 but from Experiment II.

the vertical velocity $K_{eff} \propto \hat{w}^2$ in the short-lived tracer regime (regime I, Eq. 13) and $K_{eff} \propto \hat{w}$ in the long-lived tracer regime (regime III, Eq. 17). The vertical profiles of the K_{eff} follow the scaling very well (Fig. 4). The theory also predicted that K_{eff} should be a strong function of chemical timescale (Eq. 13). This is also confirmed by the numerical simulations. K_{eff} can increase by more than a factor of 1000 from short-lived tracers to long-lived tracers (Fig. 4 and Fig. 5). This increasing trend is well predicted by our analytical theory Eq. (22). Longer-lived tracers are more dynamically controlled than chemically controlled and therefore have better correlation with the circulation pattern, leading to a larger global-mean effective vertical trans-

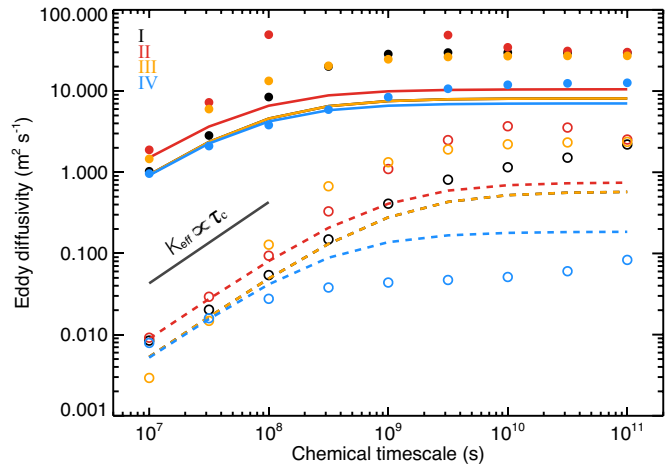


FIG. 6.— K_{eff} as a function of tracer chemical timescale for all four experiments at two typical pressure levels, 80 Pa (filled circles) and 200 Pa (open circles). The solid and dashed lines are the predictions from Eq. (22).

port. As we pointed out in Section 2, if the atmospheric dynamics is fixed (i.e., passive tracer transport), K_{eff} scales with the tracer chemical lifetime $K_{eff} \propto \tau_c$ (Eq. 13) when the tracer lifetime is short (regime I) and approaches to a constant value when the tracer lifetime is long (regime III, Eq. 17). Therefore, for tracers with very long chemical timescale, K_{eff} is insensitive to the chemical timescale (also see Eq. 22). The dependence of K_{eff} on τ_c is clearly seen in Fig. 6.

In Experiments I and II, horizontal diffusive transport via K_{yy} is small compared with the wind advection. When $\tau_c \rightarrow \infty$, the effective eddy diffusivity (Eq. 21) approaches $K_{eff} \approx Hw_0e^{nz/H}$. The analytical K_{eff} converges to a profile in Fig. 4, but does not match the numerical K_{eff} exactly. The agreement is even worse in Experiment II (Fig. 5) where the numerical K_{eff} exhibit wavy fluctuations. In the long-lived tracer regime, the derived diffusivity decreases with chemical timescale in some pressure ranges and even becomes negative at some pressure levels. This reveals a drawback in our theory in Section 2. As noted in Section 2.2.2, when the chemical lifetime is too long compared with the circulation timescale, the material surfaces of tracers are distorted significantly. The expression of K_{eff} might no longer be valid because the last term (eddy term) in the left hand side of Eq. (8), $e^z \frac{\partial}{\partial z} [e^{-z}(w\chi' - \bar{w}\chi')]$, is comparable to or even larger than the third term (mean tracer term) $w \frac{\partial \bar{\chi}}{\partial z}$ and thus it cannot be neglected. As illustrated in Fig. 7, for a short-lived tracer with $\tau_c = 10^7$ s, the eddy term is much smaller than the mean tracer term across the latitude and Eq. (22) is a good prediction of K_{eff} . But for a long-lived tracer with $\tau_c = 10^{10}$ s, the eddy term is comparable to the mean tracer term. The eddy transport is complicated in this regime and may lead to some wavy features in the numerical K_{eff} in Figs. 4 and 5, which our current analytical theory is unable to capture although the theoretical prediction is still within a factor of 2-5 in Experiment I and can be as large as a factor of 10 in Experiment II.

Note that the theoretical prediction in the long-lived tracer regime generally underestimates the eddy mixing from the numerical simulations. In this regime, the the-

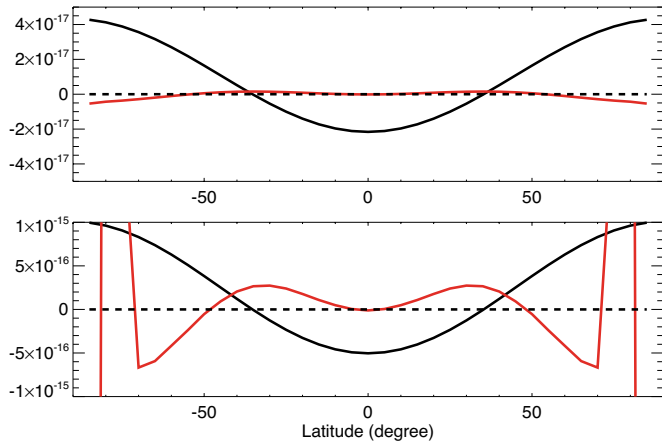


FIG. 7.— Important tracer tendency terms in Eq. (8) for a short-lived tracer (upper panel, $\tau_c = 10^7$ s) and a long-lived tracer (lower panel, $\tau_c = 10^{10}$ s) in Experiments I. The black lines represent the term $w \frac{\partial \bar{X}}{\partial z}$ and the red are $e^z \frac{\partial}{\partial z} [e^{-z} (w \chi' - \bar{w} \chi')]$.

oretical $K_{eff} \approx \hat{w} L_v$ (Eq. 17). Here we have assumed that the horizontal dynamical timescale τ_d is equal to the global advection timescale a/U and thus the vertical transport length scale $L_v \approx H$ through continuity. The discrepancy between the analytical and numerical eddy diffusivities implies that the actual horizontal dynamical timescale is larger than a/U but the mechanism is not clear. A detailed future investigation is needed.

In Experiment II (Fig. 3, third row, $\tau_c = 10^9$ s case), the overturning circulation transports the high-concentration tracers from the deep atmosphere in the southern hemisphere all the way to the top of the northern hemisphere. These tracers are then mixed downward in the northern hemisphere above 100 Pa. The global-mean mixing ratio profile of these tracers also shows a local shallow minimum at around 100 Pa (yellow line in Fig. 5). This type of local minima is also commonly found in global-mean tracer mixing ratio profiles in the simulations of convective atmospheres (see Fig. 5 in Bordwell et al. 2018). At the pressure levels right above this local minimum, because the tracer mixing ratio increases with altitude but the global-mean tracer transport is still upward, the global-mean tracer flux is against the local vertical gradient of the tracer. As a result, the predicted eddy diffusivity K_{eff} is negative above 100 Pa (Fig. 5). As we have discussed in Section 2.3.2, this type of “negative eddy diffusivity” phenomenon probably indicates that the global-mean vertical tracer transport in this case does not behave diffusively. Therefore, the diffusive assumption could break down in the long-lived tracer regime when the material surfaces are significantly distorted.

When a uniform chemical source is located at the top (Experiment III), the horizontal distribution of the tracer is anti-correlated with the vertical velocity distribution (Fig. 8), i.e., the tracer abundance is higher in the downwelling region and lower in the upwelling region, as measured on isobars. This does not alter our theory of global-mean vertical mixing in Section 2.2.1. As before, the derived effective eddy diffusivities increase with tracer chemical timescale and approaches constant in the long-lived tracer regime (Fig. 6). If we enhance the horizontal diffusion via K_{yy} (Experiment IV), the diffusion tends to

smooth out the horizontal gradient of tracer, leading to a weaker correlation between the tracer distribution and the vertical velocity. The latitudinal distribution of tracers (Fig. 8) are flatter in this case compared than that in Experiment I. The K_{eff} is thus smaller (Fig. 6) but still increases with the chemical timescale. The trend is consistent with other experiments and our theory. As seen in Fig. 6, the decrease of K_{eff} with a larger K_{yy} can also be predicted in Eq. (22).

Here we make a note on the roles of horizontal eddy diffusion and advection due to large-scale circulation. In the case with uniform chemical equilibrium abundance, vertical advection will enhance the tracer mixing slopes on an isobar while the horizontal eddy diffusion will counteract this effect by smoothing the mixing ratio variations. Therefore they have the opposite influence on the global-mean vertical tracer mixing. But the difference between the roles of horizontal advection due to the zonal-mean flow and the diffusion is subtle. In the assumption (iii) in our analytical theory (Section 2.3, and also see the Appendix), we treated both horizontal advection and horizontal diffusion in the same manner with a term of the linear relaxation form χ'/τ_d such that the horizontal dynamics always removes the horizontal mixing ratio variation (or local tracer anomaly χ') on an isobar. This is true for horizontal diffusion due to waves or irreversible turbulent eddy mixing but does not always hold for horizontal advection by the mean flow. In the mean-flow advection case, whether a local tracer anomaly is removed or enhanced essentially depends on the local convergence or divergence of the eddy tracer flux $\nabla_h \cdot (\chi' \bar{\mathbf{u}})$. The eddy tracer flux convergence does not only depend on χ' but also on the zonal-mean wind pattern $\bar{\mathbf{u}}$, or more precisely, v^* in our 2D simulations. One can show that the horizontal advection does not always relax the local tracer anomaly χ' to zero. For a crude example in a 2D system, if χ' is approximately proportional to the vertical velocity w^* (Eq. 14), using the streamfunction equation (20), one can show that $\partial(w^* v^*)/\partial y$ does not always have the opposite sign of w^* . However, this subtle effect has not been considered in our theory in Section 2. Furthermore, to the first order, χ' also depends on the vertical gradient of global-mean tracer mixing ratio (Eq. 14). Because the vertical tracer distributions are different between Experiments I and III (bottom source versus top source), the influence of the horizontal advection on the eddy tracer flux $\nabla_h \cdot (\chi' \bar{\mathbf{u}})$ in the two experiments are not exactly the same, even though the circulation and horizontal diffusion K_{yy} are the same. This leads to different K_{eff} between Experiments I and III (Fig. 6). K_{eff} is larger in Experiment II than that in Experiment I due to a slightly stronger transport using ψ_B , i.e., a bit larger γ as noted in footnote 5.

3.2. 3D Simulation on Tidally Locked Planets

If the tracer distribution exhibits significant longitudinal inhomogeneity, tracer transport is intrinsically 3D. On a slowly rotating planet such as Venus or a tidally locked planet (not necessarily a slow-rotator), the global circulation pattern could vary from the substellar-to-anti-stellar circulation in the upper atmosphere to a fast zonal-jet circulation in a lower atmosphere (e.g., Bougher et al. 1997 for Venus, Showman et al. 2013 and Zhang & Showman 2017 for tidally locked planets). Tracer trans-

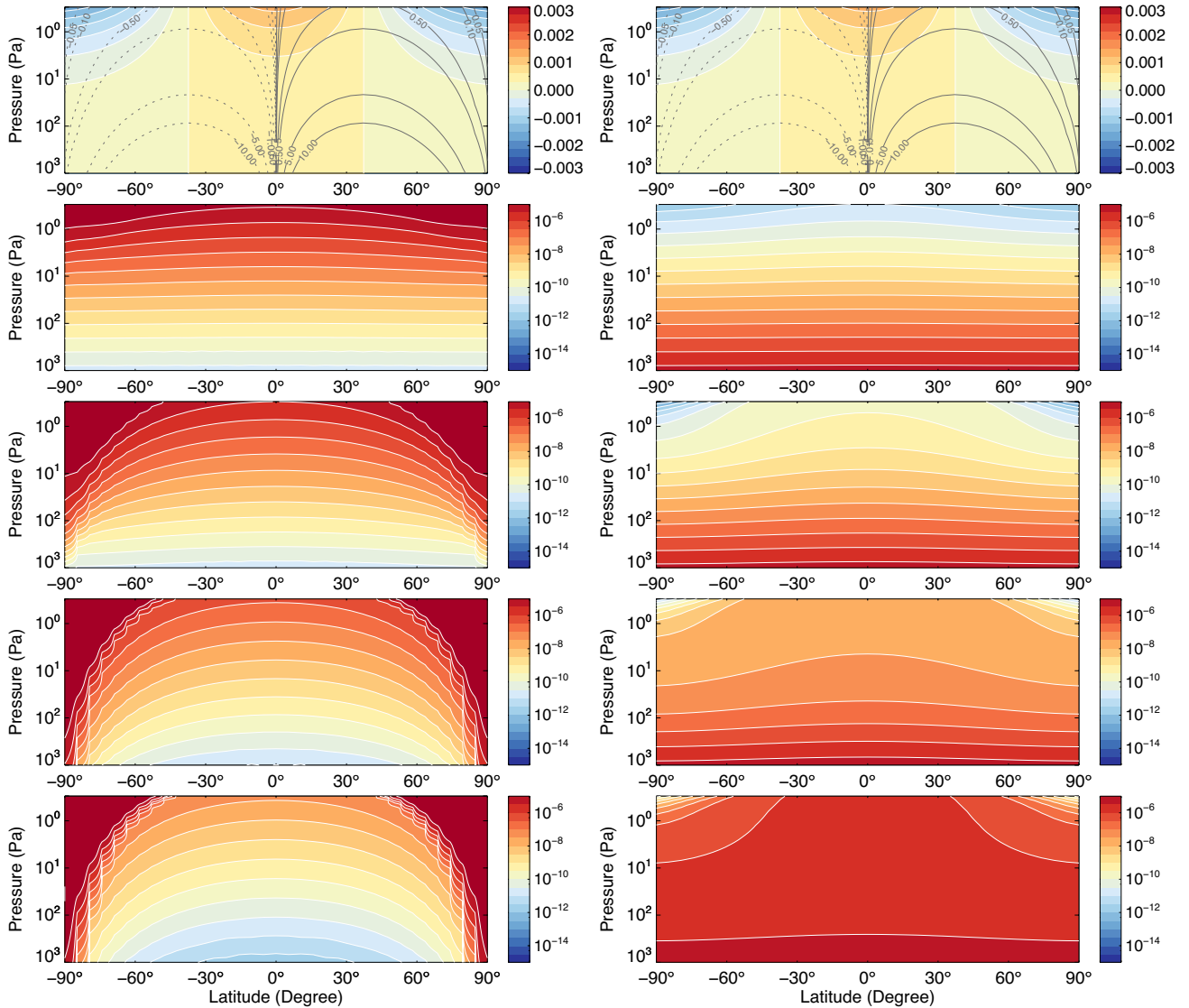


FIG. 8.— Same as Fig. 3 but for Experiments III (left) and IV (right).

port with a substellar-to-anti-stellar wind pattern cannot be treated in a 2D zonal-symmetric system as we described in Section 3.1. Even in the zonal-jet regime, the existence of longitudinally varying dynamical structures (eddies) play a critical role in both the dynamics and the mixing of chemical tracers. Moreover, the day-night temperature and insolation gradients imply that, for many tracers, there will exist large day-night variations in chemical sources and sinks that further exacerbate the longitudinal asymmetry and amplify the overall 3D nature of the problem. For instance, photochemically produced tracers on a slowly rotating planet or a tidally locked planet could develop substantially different chemistry and equilibrium tracer distributions between the dayside and nightside, a canonical example being the sulfur species from photochemistry on Venus (Zhang et al. 2012). For another example, transport of haze and cloud particles on a tidally locked planet is essentially 3D because their formation and destruction are greatly affected by the local temperature and condensable gas abundance which might have a large zonal variation. To investigate the global-mean vertical tracer transport on tidally

locked exoplanets, a 3D dynamical model is needed (e.g., Cooper & Showman 2006, Parmentier et al. 2013, Charney et al. 2015b, Lee et al. 2016).

Here we specifically focus on close-in tidally locked planets. Currently, the dominant approach of simulating the global-mean vertical distributions of chemical species and clouds on these planets is solving a 1D diffusive system with an effective eddy diffusivity and chemical/microphysical source and sinks (e.g., Moses et al. 2011, Hu et al. 2012, Tsai et al. 2017, Ackerman & Marley 2001, Helling et al. 2008, Gao & Benneke 2016). In this study we introduce passive tracers into a 3D general circulation model (GCM) and derive the effective eddy diffusivity (K_{eff}) based on the global-mean tracer distribution from simulations and the gradient-flux relationship (Eq. 6). The observable photosphere of most close-in tidally locked planets such as hot Jupiters is stratified due to the strong irradiation from the host stars. The atmospheric dynamics is approximately governed by the hydrostatic primitive equations (e.g., Showman et al. 2009). In pressure (p) coordinates, the equations includ-

ing tracer transport are:

$$\frac{D\mathbf{u}}{Dt} + f\hat{\mathbf{k}} \times \mathbf{u} + \nabla_p \Phi = F_d \quad (23a)$$

$$\frac{\partial \Phi}{\partial p} = -\frac{1}{\rho} \quad (23b)$$

$$\nabla_p \cdot \mathbf{u} + \frac{\partial \omega}{\partial p} = 0 \quad (23c)$$

$$\frac{DT}{Dt} - \frac{\omega}{\rho c_p} = \frac{q}{c_p} \quad (23d)$$

$$p = \rho RT \quad (23e)$$

$$\frac{\partial \chi}{\partial t} + \mathbf{u} \cdot \nabla_p \chi + \omega \frac{\partial \chi}{\partial p} = S \quad (23f)$$

where ρ is density; T is temperature; c_p is the heat capacity at constant pressure in units of $\text{J Kg}^{-1} \text{K}^{-1}$; R is gas constant in units of $\text{J Kg}^{-1} \text{K}^{-1}$; $\Phi = gz$ is geopotential where g is gravitational acceleration assumed constant in our study; z is altitude; $f = 2\Omega \sin \phi$ is Coriolis parameter where Ω is the planetary rotation rate and ϕ is latitude; ∇_p is the horizontal gradient at constant pressure; $\omega = Dp/Dt$ is vertical velocity in pressure coordinate that can be converted to vertical velocity in the log-pressure coordinate w ; $\mathbf{u} = (u, v)$ is the horizontal velocity at constant pressure where u is the zonal (east-west) velocity and v is the meridional (north-south) velocity; q is the radiative heating/cooling rate. $D/Dt = \partial/\partial t + \mathbf{u} \cdot \nabla_p + \omega \partial/\partial p$ is the material derivative; F_d is a drag term representing the missing physics such as magnetohydrodynamics (MHD) drag or sub-grid turbulent mixing (e.g., Li & Goodman 2010; Youdin & Mitchell 2010). χ is the mixing ratio of a tracer with chemical source/sink S .

For simplicity, we consider a planet with zero obliquity in a circular orbit around its host star. We adopt the radius, mass and rotation period of the canonical hot Jupiter HD209458b. Because we mainly focus on the tracer transport by atmospheric dynamics instead of the general circulation itself, our model setup of the dynamical forcing and damping is essentially the same as that in Liu & Showman (2013). We adopt the Newtonian cooling approximation as a simple radiative heating and cooling scheme, which, when the radiative equilibrium temperature structure and timescale are appropriately chosen, has been shown to produce wind patterns on hot Jupiters (Liu & Showman 2013) similar as that from GCMs with a realistic radiative transfer scheme (e.g., Showman et al. 2009). The heating term in Eq. (23d) is formulated as:

$$\frac{q}{c_p} = \frac{T_{eq} - T(t)}{\tau_{rad}}. \quad (24)$$

Motivated by earlier studies using Newtonian cooling (e.g., Liu & Showman 2013, Komacek & Showman 2016, Zhang & Showman 2017), we assume that the vertical profile of radiative timescale as $\tau_{rad} = 10^6(p/p_0)^{0.4}$ with $p_0 = 5 \times 10^6$ Pa. τ_{rad} ranges from 10^4 s at top to 10^6 s near the bottom (Fig. 9).

The spatial distribution of the radiative equilibrium

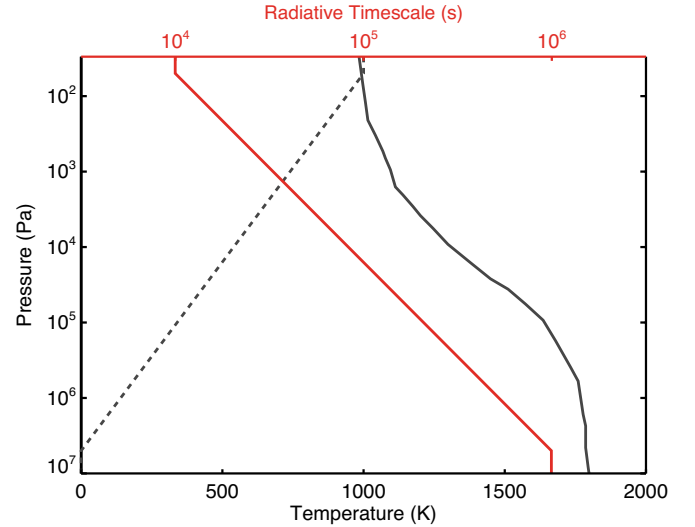


FIG. 9.— Vertical profiles of the reference temperature (black), radiative timescale (red) and a typical day-night temperature difference (ΔT_{eq} , dashed) in 3D simulations.

temperature T_{eq} is given by:

$$T_{eq}(\lambda, \phi, p) = \begin{cases} T_n(p) + \Delta T_{eq}(p) \cos \lambda \cos \phi & \text{dayside} \\ T_n(p) & \text{nightside} \end{cases} \quad (25)$$

where λ is longitude and we assume a homogeneous equilibrium temperature in the nightside $T_n(p) = T_0(p) - \Delta T_{eq}(p)/2$. The equilibrium temperature difference ΔT_{eq} is 1000 K at the top of the atmosphere and linearly decreases towards zero at the bottom in the log-pressure coordinate (Fig. 9). The mean temperature T_0 is calculated using a simplified radiative scheme from Cooper & Showman (2005).

We assume a linear drag scheme in the momentum equation (Eq. 23a), $F_d = \mathbf{u}/\tau_{drag}$. The drag coefficient (τ_{drag}^{-1}) is assumed as 0.1 day^{-1} at the bottom of the domain (10^7 Pa) and decreases linearly with decreasing pressure to zero at 5×10^5 Pa, above which the atmosphere is essentially drag-free.

As in the 2D simulations, we adopt a linear chemical scheme which relaxes the tracer distribution towards local chemical equilibrium χ_0 (Eq. 9). Here we performed a single 3D dynamical simulation with three sets of passive chemical tracers. We have 11 tracers in each set as an experiment. In other words, in the system of Equations (23), the tracer equation (23f) is actually 33 distinct equations for all tracers. Each tracer is fully and self-consistently coupled to the exact same dynamical wind pattern, but because they are passive, the tracers do not affect the dynamics, and moreover the tracers are all independent of each other, and do not interact. Therefore, one can conceptually view the dynamics, and any given single tracer, as a coupled chemical-dynamical simulation that shows how that tracer would behave, under the influence of the 3D advection field along with the tracer sources and sinks.

The design of the three sets of tracers are summarized in Table 2. In the first set (“Standard Experiment”), tracers are advected from the deep atmosphere and the distribution of χ_0 is assumed to be horizontally uniform

TABLE 2
3D TRACER CHEMICAL-DYNAMICAL SIMULATION CASES.

Experiment	Tracer	χ_0	Chemical Timescale
Standard Experiment	Deep source	Uniform	$10^{1.5+0.5i}$ s $i = 1, \dots, 11$
Quench Experiment	Deep source	Uniform	Increase towards top
Photochemical Experiment	Top source	Non-uniform	$10^{1.5+0.5i}$ s $i = 1, \dots, 11$

across the globe. We introduce 11 passive tracers of differing chemical timescale τ_c (Eq. 9) of the i th tracer is set as $\tau_c = 10^{1.5+0.5i}$ s with i from 1 to 11. The chemical timescale is assumed constant with altitude. The vertical profile of χ_0 is a power function of pressure $\chi_0 = 10^{-4}(p/p_0)^{1.6}$ with $p_0 = 5 \times 10^6$ Pa. It starts from 10^{-4} at bottom and decreases towards 10^{-12} near the top.

In the second tracer set (“Quench Experiment”), we investigate how the tracers are dynamically quenched as they are transported upward from the deep atmosphere. The tracer distribution under chemical equilibrium χ_0 is the same as the “standard case”, i.e., uniform across the globe and decreases towards upper atmosphere. But in this case the chemical timescales of the tracers are relatively long compared with tracers in the Standard case and also increase linearly with decreasing pressure in the log-pressure coordinate. The chemical timescale is fixed as 10^4 s at 5×10^6 Pa and that of the i th tracer is set as $\tau_c = 10^{5.5+0.5i}$ s at 50 Pa.

In the third tracer set (“Photochemical Experiment”), we simulate photochemically produced species produced in the upper atmosphere on the dayside. A non-uniform chemical equilibrium abundance is prescribed with a significant day-night contrast and with the day-side chemical-equilibrium abundance maximizing at high altitude:

$$\chi_0(\lambda, \phi, p) = \begin{cases} \chi_n + \Delta\chi_{eq}(p) \cos \lambda \cos \phi & \text{dayside} \\ \chi_n & \text{nightside} \end{cases} \quad (26)$$

where $\chi_n = 10^{-12}$ is the equilibrium mixing ratio on the nightside, which is taken constant here. The equilibrium tracer mixing ratio $\Delta\chi_{eq} = 10^{-12}(p/p_0)^{-1.6}$ where $p_0 = 5 \times 10^6$ Pa. $\Delta\chi_{eq}$ at the substellar point is 10^{-4} near the top of the atmosphere and decreases towards 10^{-12} at the bottom. The tracer chemical timescales are set the same as the Standard case and constant with pressure.

We simulate the atmospheric circulation and tracer transport using the MITgcm (Adcroft et al. 2004) dynamical core that solves the primitive equations using the finite volume method on a cubed sphere grid. MITgcm has been extensively used in studying atmospheric dynamics on planets (e.g., Adcroft et al. 2004; Lian & Showman 2010; Showman et al. 2009; Kataria et al. 2014) and passive tracer transport on a tidally locked exoplanet (Parmentier et al. 2013). The horizontal resolution of our simulations is C64 on a cubed sphere grid, corresponding to 256×128 in longitude and latitude, or 1.4° per grid cell. We also tested some cases using the C128 grid, corresponding to a global resolution of approximately 512×256 in longitude and latitude, or 0.7° per grid cell. The results are consistent with our lower-resolution runs. We use 80 levels from about 10^7 Pa

to 30 Pa, evenly spaced in log pressure. The time step is 20 second. We apply a fourth-order Shapiro filter to the time derivatives of horizontal velocities and potential temperature with a damping time-scale of 25 second to ensure the numerical stability. The passive tracer transport is solved using a second-order flux-limiter advection scheme. The simulations were performed for at least 5000 Earth days in model time so that the statistical properties discussed here have reached the equilibrated state. All variables were averaged over the last 400 days for analysis.

3.2.1. Results: Standard Experiment

Under a steady day-night forcing, the 3D wind pattern from our simulations is consistent with previous studies on typical hot Jupiters (e.g., Showman et al. 2009). In the east-west direction, an equatorial super-rotating wind reaches 3 to 4 km s⁻¹ at about 3000 Pa (Fig. 10). A weak westward wind develops at high latitudes on the nightside. In the north-south direction, a large-scale meridional wind blows from low latitude to the high latitude on the dayside, and the flow returns to the low latitude on the nightside (Fig. 10). The magnitude of the meridional wind is about several hundred m s⁻¹.

At low latitudes, an outstanding feature of the vertical wind pattern is the adjacent strong upwelling and downwelling flows on the nightside between the east terminator and the substellar point, i.e., longitude between 90 to 180 degrees (Fig. 10). The upwelling and downwelling flows correspond to the local divergence and convergence of the horizontal flows. A typical upwelling flow forms a chevron-like pattern tilted towards the northwest-southeast direction in the northern hemisphere and towards the southwest-northeast direction in the southern hemisphere. Surrounding the upwelling flows are the downwelling flows with a magnitude up to 20-40 m s⁻¹. In the region between longitudes -60 and 60 degrees, the dayside is dominated by a large, weaker upwelling flow pattern in both the northern and southern hemispheres. Correspondingly, the meridional wind flows away from equator with an accelerating speed that maximized at high latitude, leading to a large-scale divergence in the dayside (Fig. 10). The advection timescale due to the strong equatorial super-rotating wind a/U is on the order of 10^4 s, and that due to the meridional wind a/V is on the order of 10^5 s.

A very short-lived species generally exhibits small spatial deviations from their uniform equilibrium distribution. As predicted in Eq. (14), the spatial distribution of a short-lived tracer follows the vertical velocity pattern (Fig. 10). Two large-scale positive anomalies are located in the northern and southern hemispheres on the dayside, respectively. Adjacent positive and negative anomalies are found near the equatorial region on the nightside between the east terminator and the substellar point, corre-

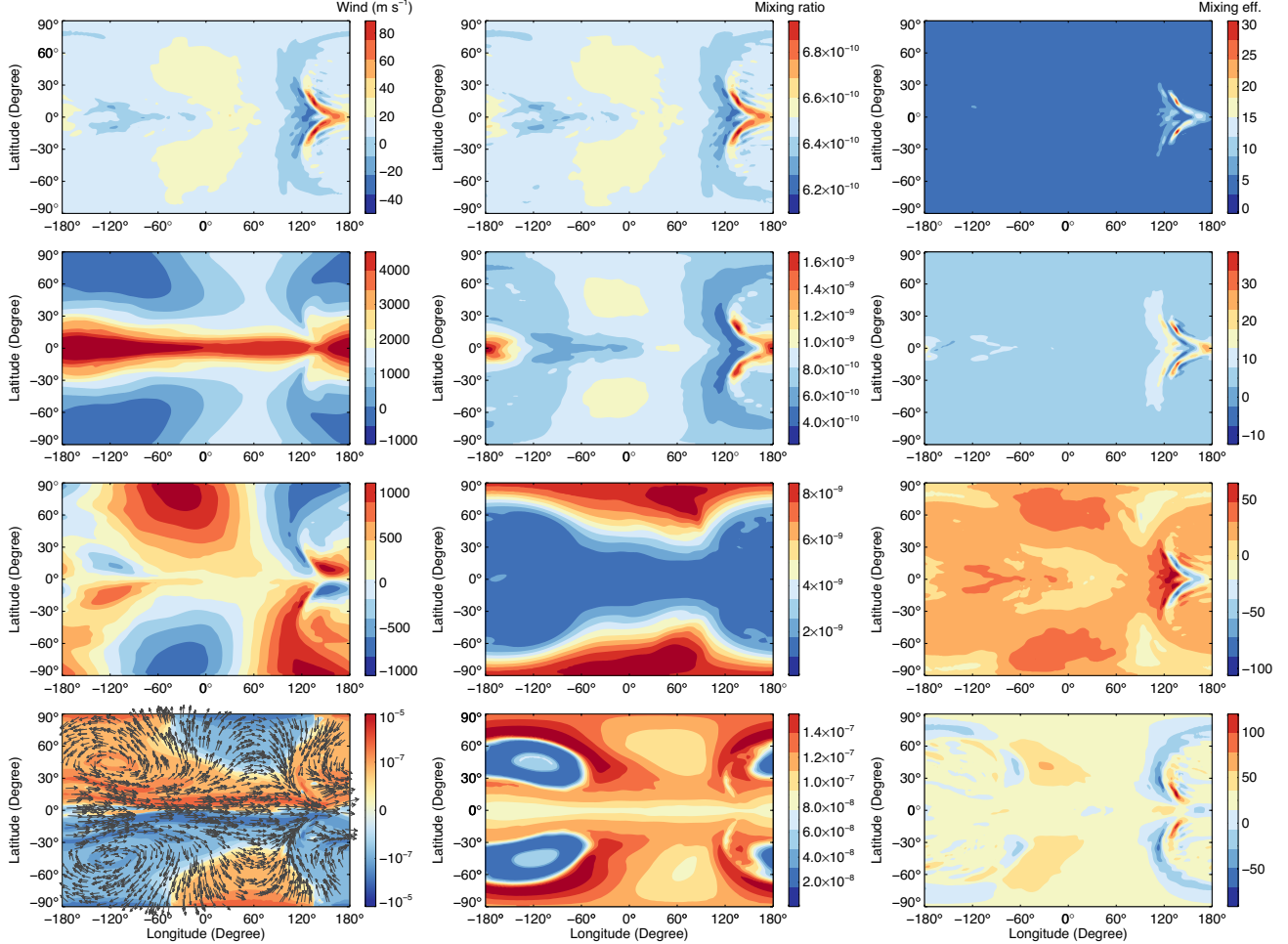


FIG. 10.— Longitude-latitude maps of various quantities at 2800 Pa in the Standard Experiment. Left column from top to the bottom: vertical wind (w), east-west wind (u), north-south wind (v), and relative vorticity (ζ) with wind field vectors. Central column: volume mixing ratios of tracers with chemical timescale of $10^{2.5}$ s, 10^4 s, $10^{5.5}$ s, 10^7 s from top to the bottom, respectively. Right column: corresponding vertical mixing efficiency of the tracers in the central column. Note that the color bars do not have the same range.

sponding to the upwelling and downwelling flows, respectively. As the chemical lifetime of the species increases, the correlation between the tracer and vertical velocity pattern becomes weaker. For species with a chemical timescale longer than advection timescales ($10^4 - 10^5$ s), the tracer tends to accumulate in the middle and high latitudes. Its longitudinal variation is generally homogenized and is much smaller than the latitudinal variation (Fig. 10). However, the very long-lived species ($\tau_c > 10^7$ s) is not homogeneously distributed across the globe. Instead, the horizontal tracer distribution exhibits some similarities with that of the relative vorticity $\zeta = \nabla \times \mathbf{u}$ where \mathbf{u} is the horizontal wind velocity vector. (Fig. 10, bottom row), suggesting the spatial pattern of inert tracer is significantly controlled by the horizontal flow pattern.

To quantify the local contribution of vertical tracer transport, we calculate the “mixing efficiency” η for each tracer (Parmentier et al. 2013):

$$\eta = \frac{w\chi - \overline{w\chi}}{\overline{w\chi}}. \quad (27)$$

Note that $\overline{w\chi} = \overline{w\chi'}$ is the global-mean vertical tracer flux. η represents the deviation of the local tracer flux from the global mean and normalized by the mean value.

For a short-lived species, due to the strong correlation between the tracer and vertical velocity, mixing efficiency is positive everywhere on an isobar (Fig. 10). η strongly maximizes at the equator on the nightside between the east terminator and the anti-stellar point, producing localized plumes or “tracer chimneys” (Parmentier et al. 2013). That the vertical tracer transport is significantly controlled by the local upwelling and downwelling plumes on tidally locked planets is consistent with Parmentier et al. (2013). However, as the tracer chemical lifetime increases, vertical mixing becomes a bit complicated. First, negative η emerges due to imperfect correlation (or some local anti-correlation) between the tracer distribution and vertical velocity. Second, the localized “tracer chimneys” where efficient transport takes place across isobars in the short-lived tracer regime become less pronounced as the tracer becomes longer-lived (Fig. 10). Interestingly, the strong upwelling plume near the east terminator, which is mostly responsible to the upward mixing for short-lived species, turns to cancel the upward mixing in the long-lived species case as the horizontal tracer distribution changes with the tracer chemical lifetime (Fig. 10).

The zonally averaged vertical velocity and tracer abundance are shown in Fig. 11. The zonal-mean circulation

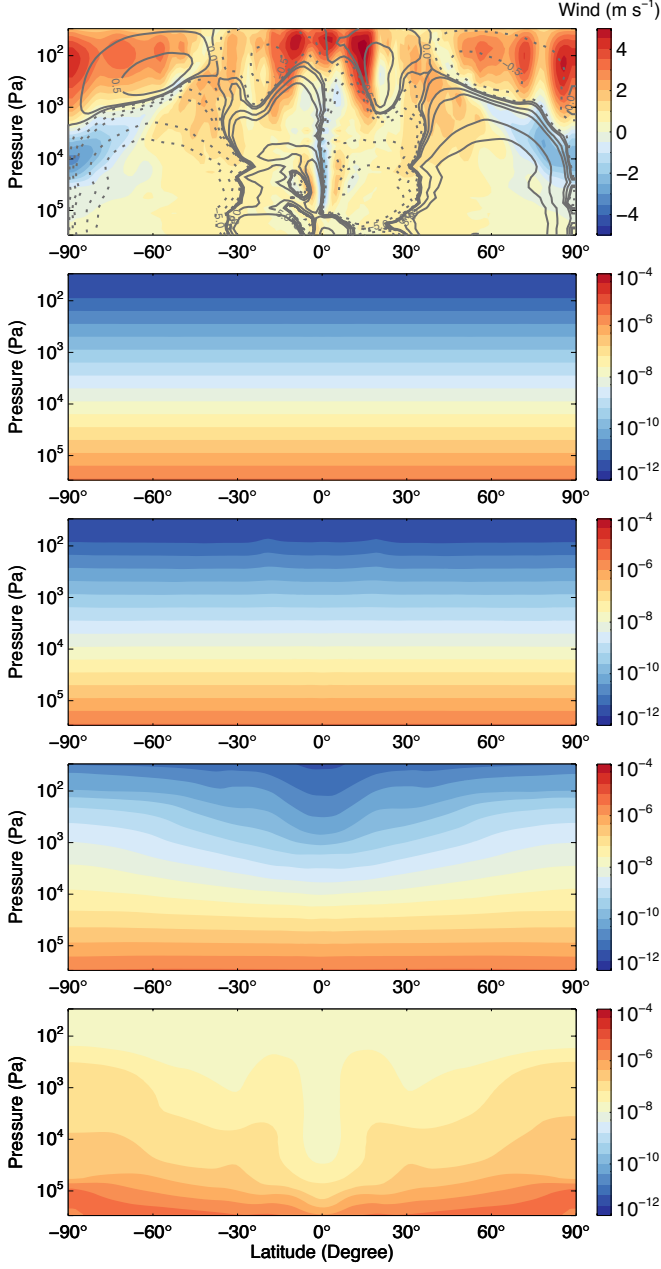


FIG. 11.— Latitude-pressure maps of zonally averaged quantities in the Standard Experiment. Top: vertical wind velocity (color) and TEM mass streamfunction (contours, in units of $10^{12} \text{ Kg s}^{-1}$, solid/positive is clockwise). Starting from the second row we show volume mixing ratio of tracers with different chemical timescales of 10^2 s , $10^{3.5} \text{ s}$, 10^5 s , $10^{6.5} \text{ s}$ from top to bottom, respectively.

exhibits a net downwelling at equator with two strong upwelling regions near the equator. The polar regions are mostly downwelling. Correspondingly, the Transformed Eulerian Mean (TEM) streamfunction exhibits two “anti-Hadley cells” in the equatorial region⁶. Two more circulation cells exist with ascending branches at middle latitudes and descending branches at high lati-

⁶ This result seems consistent with a recent Super-Earth study by Charnay et al. (2015a). But here we emphasize that whether this “anti-Hadley” circulation occurs depends on the parameters in the setup. Some hot Jupiter simulations do not show this feature (personal communications with V. Parmentier)

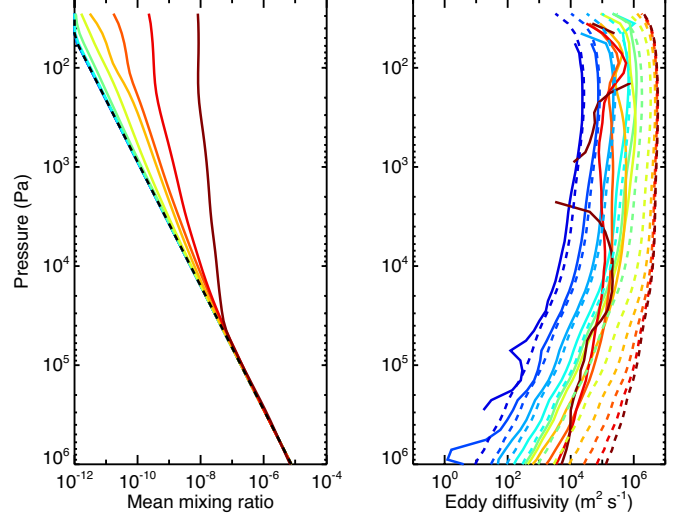


FIG. 12.— Left: Vertical profiles of the global-mean volume mixing ratio in the Standard Experiment. Right: vertical profiles of numerically derived effective eddy diffusivity K_{eff} (right) from the flux-gradient relationship (Eq. 6) based on simulations (solid) and that from an analytical prediction (dashed) from Eq. (28) with $L_v \sim H$ and \hat{w} from the simulation. Different colors from cold (blue) to warm (red) represent tracers with different chemical timescales from short to long, ranging from 10^2 s to $10^{6.5} \text{ s}$.

tudes. As a result, the zonal-mean distribution of long-lived tracers exhibits a local minimum near the equator in our simulations (Fig. 11).

Similar to the 2D model results, the global-mean tracer mixing ratio profile is close to the chemical equilibrium if the chemical timescale is short and becomes more vertically homogenized as the tracer lifetime increases (Fig. 12). A detailed discussion of the departure of the tracer vertical profile from its chemical equilibrium profile will be presented later in the “Quench Experiment”.

Based on the simulation results, we numerically derived effective eddy diffusivities K_{eff} from the flux-gradient relationship (Eq. 6). K_{eff} increases with decreasing pressure as the vertical velocity also increases. K_{eff} increases with chemical timescale, spanning over 3-4 orders of magnitude. However, as also seen in the 2D simulations, for long-lived species, the dependence of K_{eff} on chemical lifetime is complicated. At some pressure (e.g., 2000 Pa), as the tracer lifetime increases, K_{eff} actually decreases in this regime. Again, this behavior can be understood owing to the fact that the material surfaces of the tracer have been significantly distorted in the case of long-lived species. The correlation between the vertical velocity and tracer is not good (Fig. 10) and eventually our theory in Section 2 based on relatively short-lived species fails in this regime.

We also analytically predict K_{eff} based on the theory in Section 2. Unlike the earlier discussion for the 2D model in Section 3.1, here we could estimate horizontal mixing due to the resolved dynamics, because the large-scale dynamics likely does cause horizontal mixing in our fully resolved 3D simulations. First, we estimated the horizontal transport timescale τ_d and vertical velocity scale \hat{w} . We assume the horizontal tracer mixing is only due to large-scale horizontal transport. From the continuity equation, τ_d can also be estimated from the vertical dynamical timescale $\tau_d = L_h/U \approx L_v/\hat{w}$, where \hat{w} is the vertical velocity scale. As this is a uniform χ_0

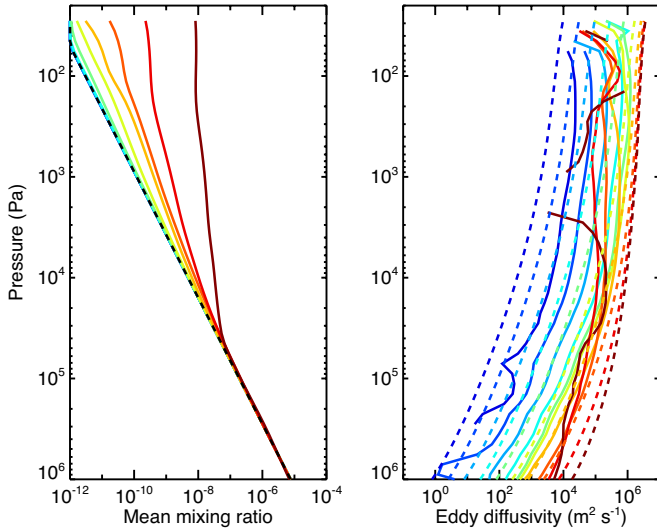


FIG. 13.— Same as Fig. 12 but the predicted K_{eff} (dashed) is calculated using Eq. (28) with $L_v \sim H$ from our analytical theory of vertical velocity from Eq. (32).

case in regime I, the non-diffusive term vanishes. K_{eff} can then be obtained from Eq. (13):

$$K_{eff} \approx \frac{\hat{w}^2}{\hat{w}/L_v + \tau_c^{-1}}. \quad (28)$$

We estimated \hat{w} using the root-mean-square of vertical velocity across the globe from our simulations. We take the vertical characteristic length scale L_v as the pressure scale height H , which is equivalently to assuming typical horizontal length scale L_h as the planetary radius a according to the continuity equation $U/a \sim \hat{w}/H$ (Komacek & Showman 2016). Eq. (28) gives a good prediction of K_{eff} (Fig. 12). Our theory in Section 2 is applied well to the regime of 3D atmospheres on close-in tidally locked exoplanets with a deep uniform chemical equilibrium abundance.

As in the 2D prediction (Fig. 8), our theory does not perform well in long-lived tracer regime where the tracer contours are significantly distorted. But the 3D results are different from the 2D cases in which the analytical K_{eff} generally underestimates the numerical eddy mixing. In the 3D simulations, our theory generally overestimates K_{eff} . Again, the reason could be the adopted tracer transport length scale here—we have assumed $L_v \sim H$ and $L_h \sim a$. But as shown in the mixing efficiency maps (Fig. 10), strong local tracer transport could dominate the entire globe, implying a smaller L_h . As also mentioned in Section 2.4, in the long-lived tracer regime (regime III), L_v might be different from the atmospheric scale height H . Previous studies (e.g. Cooper & Showman 2006) have pointed out that L_v for CO transport on hot Jupiters might be a factor of 2-3 smaller than H . If we adopt a smaller dynamical length scale, the resultant K_{eff} would be smaller and match the 3D numerical results better in the long-lived tracer regime.

We also go one step further to predict the vertical velocity scale \hat{w} from first principles (i.e., not based on the numerical simulations). This might be achieved using the scaling theory developed in Komacek & Showman (2016) and Zhang & Showman (2017). First, the horizontal velocity scale U can be approximated as (see Appendix A in

Zhang & Showman 2017):

$$\frac{U}{U_{eq}} \sim \sqrt{(\alpha/2\gamma)^2 + 1} - \alpha/2\gamma \quad (29)$$

where the non-dimensional parameters α and γ are defined as:

$$\alpha = 1 + \frac{(\Omega + \tau_{drag}^{-1})\tau_{wave}^2}{\tau_{rad}\Delta \ln p} \quad (30)$$

$$\gamma = \frac{\tau_{wave}^2}{\tau_{rad}\tau_{adv,eq}\Delta \ln p}. \quad (31)$$

Here $\tau_{wave} \sim L/NH$ is the wave propagation timescale over a typical horizontal dynamics length scale L and N is the buoyancy frequency (Brunt-Väisälä frequency) of the atmosphere. $\tau_{adv,eq} \sim L/U_{eq}$ is the advective timescale due to the “equilibrium cyclostrophic wind” $U_{eq} = (R\Delta T_{eq}\Delta \ln p/2)^{1/2}$.

With the analytical expression of U , we can predict the \hat{w} . We assume the typical horizontal length scale $L \sim a$ and the continuity equation states $U/a \sim \hat{w}/H$ (Komacek & Showman 2016). The vertical velocity scale \hat{w} can be estimated as:

$$\hat{w} \sim \frac{U_{eq}a}{H} (\sqrt{(\alpha/2\gamma)^2 + 1} - \alpha/2\gamma). \quad (32)$$

Insert Eq. (32) into Eq. (28) and we obtain the analytical K_{eff} for tidally locked exoplanets from first principles. In general using Eq. (32) in Eq. (28) and assuming $L_v \sim H$ provides good prediction of the K_{eff} profiles. Similar to the numerically derived K_{eff} , the predicted K_{eff} (Fig. 13) increases with the chemical lifetime and with decreasing pressure. For most tracers, the analytical K_{eff} matches well with the K_{eff} derived from the simulations. But our theory underestimates the numerical K_{eff} by about a factor of 10 for short-lived tracers. This discrepancy is because both the horizontal (Eq. 29) and vertical (Eq. 32) velocities estimated from our analytical theory are less by about factor of 2-3 than the numerical values in a drag-free hydrogen atmosphere (Komacek & Showman 2016, Zhang & Showman 2017). As the K_{eff} scales with the vertical velocity square for the short-lived tracers (Eq. 28), the K_{eff} predicted by our theory is about 10 times smaller than that from 3D models. When the drag is applied in the model, the analytical K_{eff} matches better with the numerical simulations (personal communication with T. Komacek).

3.2.2. Results: Quench Experiment

For tracers that are transported from deep atmospheric sources, their mixing ratios can be vertically homogenized by the atmospheric dynamics and “quenched” at a value at a deeper pressure level (Fig. 14). This usually occurs when the chemical timescale of the tracer changes significantly with pressure. For example, high temperature in the deeper atmosphere maintains fast thermochemical reactions of a tracer and results in a short chemical timescale. Chemistry dominates over the dynamics and the tracer is expected to be in local thermochemical equilibrium. As the tracer is advected upward, chemical reactions slow down as the temperature decreases in the upper atmosphere, and the chemical timescale increases quickly. At a certain pressure level, the vertical profile

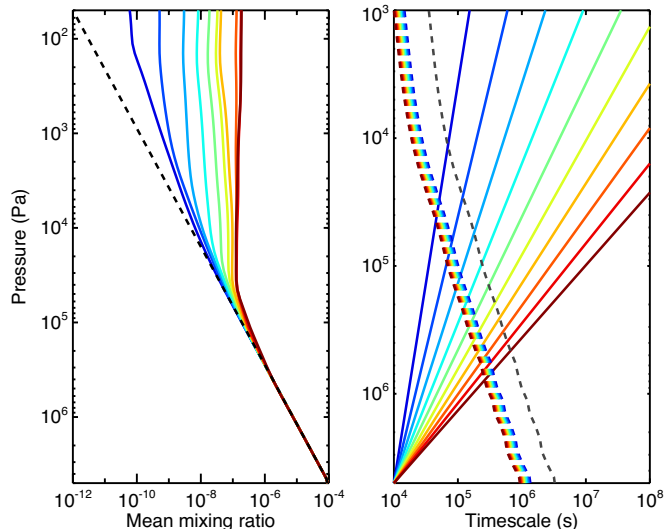


FIG. 14.— Left: vertical profiles of the global-mean volume mixing ratio from numerical simulations (solid) and the equilibrium mixing ratio (dashed) in the Quench Experiment. Right: vertical profiles of the chemical lifetimes (solid) and vertical transport timescales based on pressure scale height (black dashed) and equilibrium chemical scale height for individual tracers (color dashed). Different colors from cold (blue) to warm (red) represent tracers with different chemical timescales from short to long.

of the chemical tracer starts to depart from its chemical equilibrium profile. Above that level, the tracer will be more controlled by the atmospheric dynamics. If the tracer chemical timescale increases so rapidly with decreasing pressure that the chemistry can be quickly neglected above the departure level (e.g., carbon monoxide on Jupiter, Prinn & Barshay 1977), the tracer mixing ratio in the upper atmosphere is approximately constant and is basically set by the value at the departure level. This is called quenching.

One can define two kinds of “quench points” (Bordwell et al. 2018). The first one is the “departure quench point”, which stands for the pressure level where the tracer vertical profile starts to deviate from the chemical equilibrium tracer profile. The second one is the “observed quench point”, referring to a pressure level at which the equilibrium tracer mixing ratio is equal to the tracer mixing ratio in the upper atmosphere. The two quench points are the same if the tracer mixing ratio profile becomes vertically constant quickly as it deviates from the equilibrium profile (e.g., red line in Fig. 14). On the other hand, if the chemical timescale does not increase very quickly and the chemistry above the departure point cannot be neglected, the tracer mixing ratio will keep decreasing and may not reach a constant vertical profile until in the very top atmosphere (e.g. blue line in Fig. 14). In this case, the two quench points are not the same. In this study we mainly focus on the departure quenching point.

Dynamical quenching of the disequilibrium chemical tracers is usually investigated in the convective atmospheres (e.g., Prinn & Owen 1976, Prinn & Barshay 1977, Smith 1998, Visscher & Moses 2011, Bordwell et al. 2018). However, in the radiative zone of the atmospheres on tidally locked planets with rigorous vertical transport, dynamical quenching of long-lived species such as H_2O , CH_4 and CO is also important (e.g., Cooper & Showman

2006, Moses et al. 2011, Line et al. 2011). In the Quench Experiment, the tracer chemical timescales increase with decreasing pressure and span many orders of magnitude (Fig. 14). The chemical timescale of the longest-lived tracer has a very steep vertical gradient, ranging from 10^4 s at 5×10^6 Pa to 10^{11} s at 50 Pa. The departure point of this tracer from the equilibrium chemical profile is at 4×10^5 Pa and the “observed” quench point is roughly at 10^5 Pa (Fig. 14). The chemical timescale of the shortest-lived tracer ranges from 10^4 s at 5×10^6 Pa to 10^6 s at 50 Pa. The departure point is at about 6×10^4 Pa. But the tracer mixing ratio decreases with pressure towards the top of the atmosphere because the local chemistry plays a non-negligible role in all pressure range. There is no clear “observed quench point” for this tracer case.

To understand the details of the dynamical quenching in the atmosphere of a 3D tidally locked planet, we analyzed a typical long-lived tracer with a quenched vertical profile (orange line in Fig. 14). The chemical timescale of this tracer ranges from 10^4 s at 5×10^6 Pa to $10^{9.5}$ s at 50 Pa. The departure point of this tracer is at about 3.6×10^5 Pa and the “reflection point”, where the tracer vertical profile becomes vertically constant, is at about 5.7×10^4 Pa (Fig. 14). We plotted the spatial maps of vertical wind and tracer mixing ratio at several typical pressure levels (Fig. 15), including an upper atmosphere level (9×10^3 Pa) above the reflection point and a deep atmosphere level (1.4×10^6 Pa) below the departure point.

There are many similarities in the spatial distributions between Fig. 15 for this typical tracer in the Quench Experiment and Fig. 10 for four different tracers with chemical timescales constant with pressure in the Standard Experiment. This implies that the spatial distributions of the tracer in the Quench Experiment can be approximately understood using its local chemical timescale. Because the tracer chemical timescale increases from bottom to the top, while the vertical transport timescale decreases, the ratio of the chemical timescale and dynamical timescale in the atmosphere τ_c/τ_d increases with decreasing pressure. As a result, the tracer in the Quench Experiment at the deep atmosphere level behaves as a short-lived tracer and that at the upper atmosphere level behaves as a long-lived tracer in the Standard Experiment.

At the deep atmospheric level, the tracer spatial distribution is similar to the vertical wind pattern, especially in the equatorial region (Fig. 15, bottom row). At the departure level, the dynamical timescale is roughly equal to the chemical timescale, tracer is more horizontally homogenized. Below the departure level, the mixing efficiency maps are generally positive in the off-equatorial region, indicating a decent correlation between the tracer distribution and the vertical wind, although at equator negative mixing efficiency appears at several locations. At the reflection point where the tracer mixing ratio stops decreasing with decreasing pressure, large positive and negative anomalies show up in the mixing efficiency map (Fig. 15), implying a large cancellation between the tracer upwelling and downwelling. The tracer is further more spatially homogeneous because atmospheric dynamics becomes more important. Above the reflection point, the tracer distribution looks similar to the typical

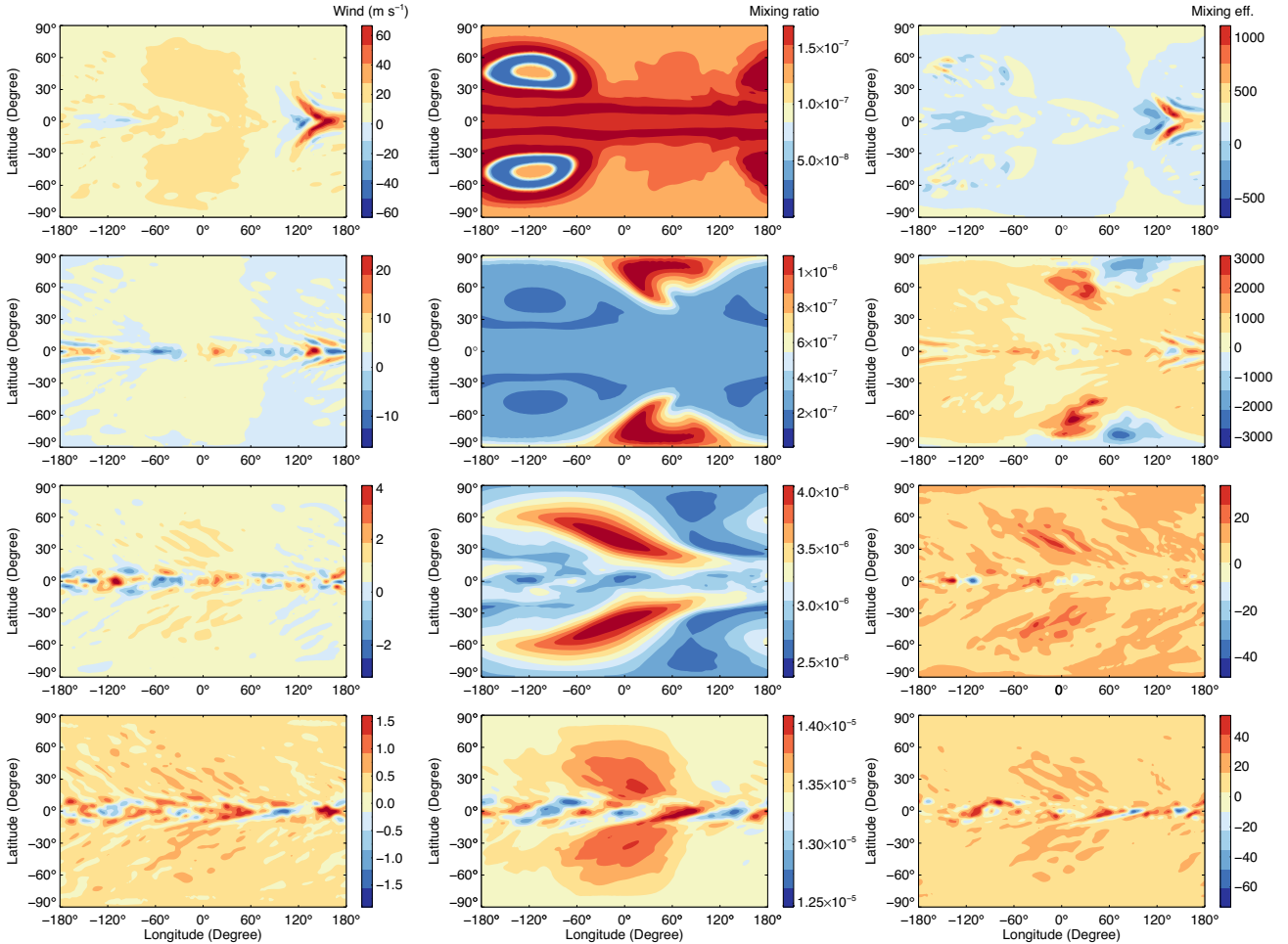


FIG. 15.— Longitude-latitude maps of vertical wind (left), tracer mixing ratios (central) and vertical mixing efficiency (right) from 3D Quench simulation of a tracer with chemical timescale $10^{9.5}$ s at 50 Pa (orange line in Fig. 14). The pressure levels from top to bottom: 9×10^3 Pa (upper atmosphere), 5.7×10^4 Pa (reflection point), 3.6×10^5 Pa (departure point), 1.4×10^6 Pa (deep atmosphere).

long-lived tracer in the Standard Experiment (Fig. 10, bottom row). Although the τ_c/τ_d is large in the upper atmosphere, the tracer is not completely homogenized. Instead, its spatial pattern is significantly affected by the horizontal wind dynamics. The local anomalies located at the mid-latitudes at around west terminator are a response to the large local wind gyres seen in the vorticity map (Fig. 10, bottom row). The upwelling and downwelling shown in the mixing efficiency map almost cancel each other, resulting in nearly zero net vertical transport flux. From the tracer continuity equation (Eq. 23f), if the local chemical source and sink were neglected ($S \approx 0$), the vertical tracer flux divergence should vanish as well. In the diffusive framework, this implies that the vertical gradient of the tracer mixing ratio is nearly zero, and the tracer profile is approximately constant with pressure (Fig. 14).

To visualize the vertical transport of this tracer, we also diagnosed the zonal-mean map and meridional-mean map of vertical wind and tracer mixing ratio (Fig. 16). In the zonal-mean maps, we simply averaged the quantities over longitude at each latitude to produce the latitude-pressure distributions. In the meridional-mean maps, at each longitude point, we averaged the quantities over latitude in an area-weighted fashion. The vertical tracer quenching occurs at a deeper atmospheric level in the

equatorial region but the quenched tracer mixing ratio is higher than the other latitudes. There appears another quenching point at around 10^4 Pa. The equatorial minimum feature in the latitude-pressure distribution is a result of the net downwelling of the lower-mixing-ratio tracers from the upper atmosphere due to the “anti-Hadley cells” in the equatorial region, as shown in the TEM streamfunction (Fig. 16). We have discussed this behavior in the Standard Experiment (Fig. 11).

In the longitudinal direction, the vertical quenching occurs at larger pressure level in the west hemisphere than in the east hemisphere (see the bottom two meridional-mean map in Fig. 16). Furthermore, the quenched tracer mixing ratio in the east hemisphere is actually higher than that in the west hemisphere. The reason is that, when the tracer is transported upward near the substellar longitude from the deep atmosphere, the equatorial superrotating wind advects the tracer to the east hemisphere and enhances the local tracer mixing ratio. This can also be considered as “horizontal quenching effect” of the tracer in the east hemisphere due to strong horizontal transport (see an earlier study in Cooper & Showman 2006).

Despite that the quenching level has some spatial variation, here we estimate the global-mean quenching level. In this study we mainly focus on the departure quench-

ing point as a more generic metric. We determined the departure points from the tracer profiles in the Quench simulations (Fig. 17). The numerical departure points are measured as the pressure level where the simulated tracer mixing ratio deviates from (larger than) the equilibrium mixing ratio by a small fraction (Fig. 14). In this study we use 1%. As the tracer mixing ratio increases very quickly above the departure point, this estimated departure point is not very sensitive to the choice of the small fraction (e.g., 10%).

Crudely speaking, quenching (or departure) occurs where the chemical timescale is equal to the vertically mixing timescale (e.g., Prinn & Barshay 1977, Cooper & Showman 2006, Visscher & Moses 2011). In the global-mean vertical eddy diffusion framework, the vertical mixing timescale is the effective diffusive timescale. In the 3D atmosphere with uniform χ_0 , Eq. (28) is a good approximation of the eddy diffusivity. As our theory of K_{eff} does not make any assumption whether τ_c should be constant with pressure or not, Eq. (28) is also applicable to the Quench Experiment in which tracer lifetime varies with pressure. Equating the chemical timescale and effective diffusion timescale at the quenching point, we can achieve:

$$\tau_c \sim \frac{L_v^2}{K_{eff}} \approx \frac{L_v}{\hat{w}} \left(1 + \frac{L_v}{\hat{w}\tau_c}\right) \quad (33)$$

where $\tau_c \sim L_v/\hat{w}$ is the traditional quenching level estimate used in the convective atmosphere (e.g., Prinn & Barshay 1977) and on hot Jupiters (e.g., Cooper & Showman 2006). Our quenching theory has an additional term that represents the effect of the tracer chemistry on the global-mean vertical tracer transport efficiency. This effect has not been addressed before because previous quenching theories did not include large-scale circulation to estimate the global-mean tracer transport. Previous studies (e.g., Smith 1998, Cooper & Showman 2006, Bordwell et al. 2018) showed that the tracer chemistry could affect the vertical characteristic length scale L_v , leading to a different departure point estimate. Following Prinn & Barshay (1977), Bordwell et al. (2018) proposed a length scale as the scale height of the tracer destruction rate under chemical equilibrium. But this length scale only depends on the vertical gradient of the chemical timescale, not the chemical timescale itself in our theory.

How does the tracer chemical timescale itself affect the quenching? From our global-mean eddy diffusivity theory, a tracer with shorter chemical timescale tends to have a smaller K_{eff} , implying less effective mixing. Because the tracer chemical timescale generally increases with decreasing pressure, the tracer quenching level in our theory should occur at lower pressure than the conventional estimate using $\tau_c \sim L_v/\hat{w}$. In other words, because the conventional theory assumes the eddy diffusivity as $\hat{w}L_v$, which is the maximum eddy diffusivity we can achieve in our theory, the conventional estimate gives an upper bound on the quenching pressure.

It looks like our quenching theory implies that different tracers should be treated individually to estimate their quenching points. But interestingly, one can solve for τ_c

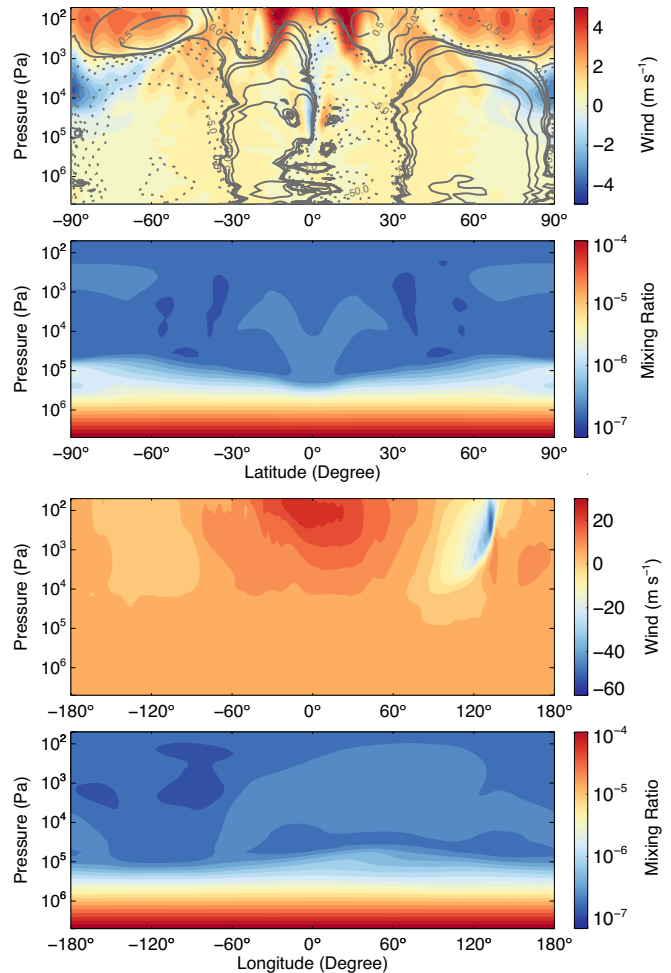


FIG. 16.— 2D maps from a typical Quench Experiment with chemical tracer timescale $10^{9.5}$ s at 50 Pa (orange line in Fig. 14). Top: zonally averaged vertical wind velocity (color) and TEM mass streamfunction (contours, in units of 10^{12} Kg s⁻¹, solid/positive is clockwise). Second: zonally averaged tracer mixing ratio. Third: area-weighted latitudinal-averaged vertical wind velocity. Bottom: area-weighted latitudinal-averaged tracer mixing ratio.

in Eq. (33) to simplify the relationship:

$$\tau_c \sim \frac{1 + \sqrt{5}}{2} \frac{L_v}{\hat{w}}. \quad (34)$$

Therefore, using the chemical-dependent eddy diffusivity, the quenching point is systematically shifted to lower pressure. Or equivalently speaking, our theory implies the traditional vertical length scale should be scaled by an additional factor, the golden ratio, to take the tracer chemistry into account. This will increase L_v by a factor of about 1.6.

Let us first assume the horizontal dynamical timescale τ_d is a/U and thus L_v is the pressure scale height H , the right hand side in Eq. (34), which we call the “effective dynamical timescale” in this study, is shown in Fig. 14. We can find out its cross point with the chemical timescale profile τ_c to predict the departure point of that species. Using the \hat{w} from the 3D simulations, the predicted departure points agree well with the longer-lived tracers in our simulations (Fig. 17). But for shorter-lived species, the predicted quenching pressure is much smaller than the model results.

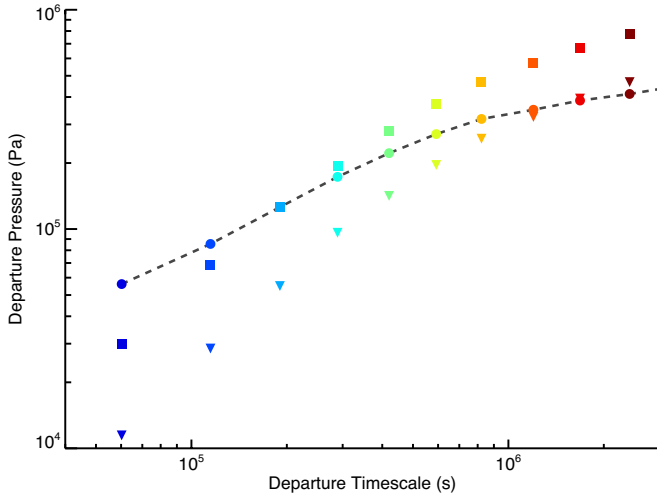


FIG. 17.— Departure points as a function of departure temperature in the Quench Experiment (dots connected by the dashed line). Theoretical predictions using our quench theory (Eq. 34) with $L_v \sim H$ (triangles) and $L_v \sim H_{ceq}$ (squares). The color scheme is the same as in Fig. 14.

It is possible that horizontal dynamical timescale is different from a/U and L_v is not the same as H . We tested the situation in which L_v is assumed as the “chemical scale height”, H_c , the scale height of the tracer chemical destruction rate that was introduced in the convective atmosphere study (Bordwell et al. 2018). As we use a simple linear chemical scheme in the Quench Experiment (Eq. 9), the chemical loss rate can be expressed as $N\bar{\chi}/\tau_c$, where N is the atmospheric number density and $\bar{\chi}$ is the global-mean vertical profile of tracer. The chemical scale height in our study is:

$$H_c = \frac{\partial \ln(N\bar{\chi}/\tau_c)}{\partial \ln p} \approx H \left(1 + \frac{\partial \ln \bar{\chi}}{\partial \ln p} - \frac{\partial \ln \tau_c}{\partial \ln p} \right) \quad (35)$$

where we have approximated the number density scale height using the pressure scale height H . In most cases, a chemical tracer does not quench to a vertically constant profile right at the departure point. We can also approximate the actual scale height of the tracer at around the departure point using the scale height of its equilibrium mixing ratio χ_{eq} . Substitute $\bar{\chi}$ with χ_{eq} in Eq. (35) and the chemical scale height H_c becomes the “equilibrium chemical scale height” H_{ceq} (Bordwell et al. 2018).

Using $L_v \sim H_{ceq}$ in Eq. (34), the “effective dynamical timescale” in Eq. (34) is species-dependent (Fig. 14). Because the equilibrium mixing ratio χ_{eq} is the same for all species, the species with a steeper vertical gradient of τ_c (also the longer-lived species in our cases) has a smaller effective dynamical timescale. In our simulations, as pressure decreases, the equilibrium mixing ratio χ_{eq} decreases and chemical timescale τ_c increases. Therefore chemical destruction rate decreases faster than the pressure (or density) decrease, and thus H_{ceq} is smaller than H . This implies a smaller effective dynamical timescale, or a more efficient vertical transport, than the case using $L_v \sim H$. The predicted quenching points are thus located in a relatively deeper atmosphere (Fig. 14 and Fig. 17). Overall, using $L_v \sim H_{ceq}$ could explain the departure points for the short-lived species but overestimates the pressure of quenching for long-lived tracers. In the latter regime, using $L_v \sim H$ gives a better prediction.

3.2.3. Results: Photochemical Experiment

Using the same dynamical field, we also investigated models where the tracer chemical equilibrium abundance varies strongly from the dayside to the nightside (Eq. 26). With a dayside chemical source, we can approximately simulate photochemically or ion-chemically produced species on tidally locked planets. The wind field and circulation have been discussed in the Standard case (Section 3.2.1). The tracer distributions look significantly different from previous cases (Fig. 18). For short-lived species, the tracer distribution is close to the prescribed chemical equilibrium distribution (Eq. 26) which maximizes at the sub-stellar point. The tracer abundance decreases away from the sub-stellar point and becomes approximately homogeneous on the nightside with a mixing ratio of 10^{-12} . As the horizontal dynamical transport might be neglected when the tracer lifetime is short ($\tau_c \ll \tau_a$), the tracer distribution in this limit can be approximated based on Eq. (11):

$$\chi' = \chi'_0 - w\tau_c \frac{\partial \bar{\chi}}{\partial z}. \quad (36)$$

In this case, it is the deviation of the tracer mixing ratio from its chemical equilibrium distribution, instead of the tracer mixing ratio itself, that is anti-correlated with the vertical velocity pattern.

As the tracer chemical lifetime increases, atmospheric dynamics plays a more important role in shaping the tracer spatial distribution. The spatial pattern exhibits a “chemical hot spot shift” on the dayside where the maximum abundance of tracer occurs slightly east of the sub-stellar point (Fig. 18). This hot spot shift pattern resembles the well-known “temperature hot spot” on tidally locked planets (e.g., Showman & Guillot 2002, Knutson et al. 2007). The chemical hot spot phase shift might also be detected by the light curve at the wavelengths where the species has significantly strong absorption or emission features. Physically, this chemical hot spot shift is a result of competition between the horizontal advection and chemical relaxation. Thus the phase shift could be predicted in a simple chemical-transport model in the longitudinal direction (Zhang et al. 2013b) with a sinusoidal chemical equilibrium distribution. That theory states that the chemical hot spot phase shift ϕ_s is determined by the ratio of the chemical relaxation timescale to the advection timescale: $\phi_s = \tan^{-1}(\tau_c U/a)$. For a tracer with lifetime $\tau_c = 10^4$ s (second row in Fig. 18), if we adopt the zonal-mean zonal wind velocity scale $U \sim 2$ km s $^{-1}$ at 2800 Pa, we predict a chemical hot spot phase shift $\phi_s \sim 10$ degrees, roughly consistent with the simulation result. A more rigorous derivation to the phase shift can adopt the approach in the Appendix B in Zhang & Showman (2017) by replacing the temperature variable and radiative timescale with the chemical mixing ratio and chemical lifetime, respectively. But the predicted phase shifts from the above two approaches are generally very close.

If the tracer lifetime is significantly longer than both the east-west and north-south advection timescales, the spatial pattern of the tracer is different from the “chemical hot spot” pattern. In our simulations, the tracers are more concentrated at low latitudes with some positive anomaly features near both terminator regions

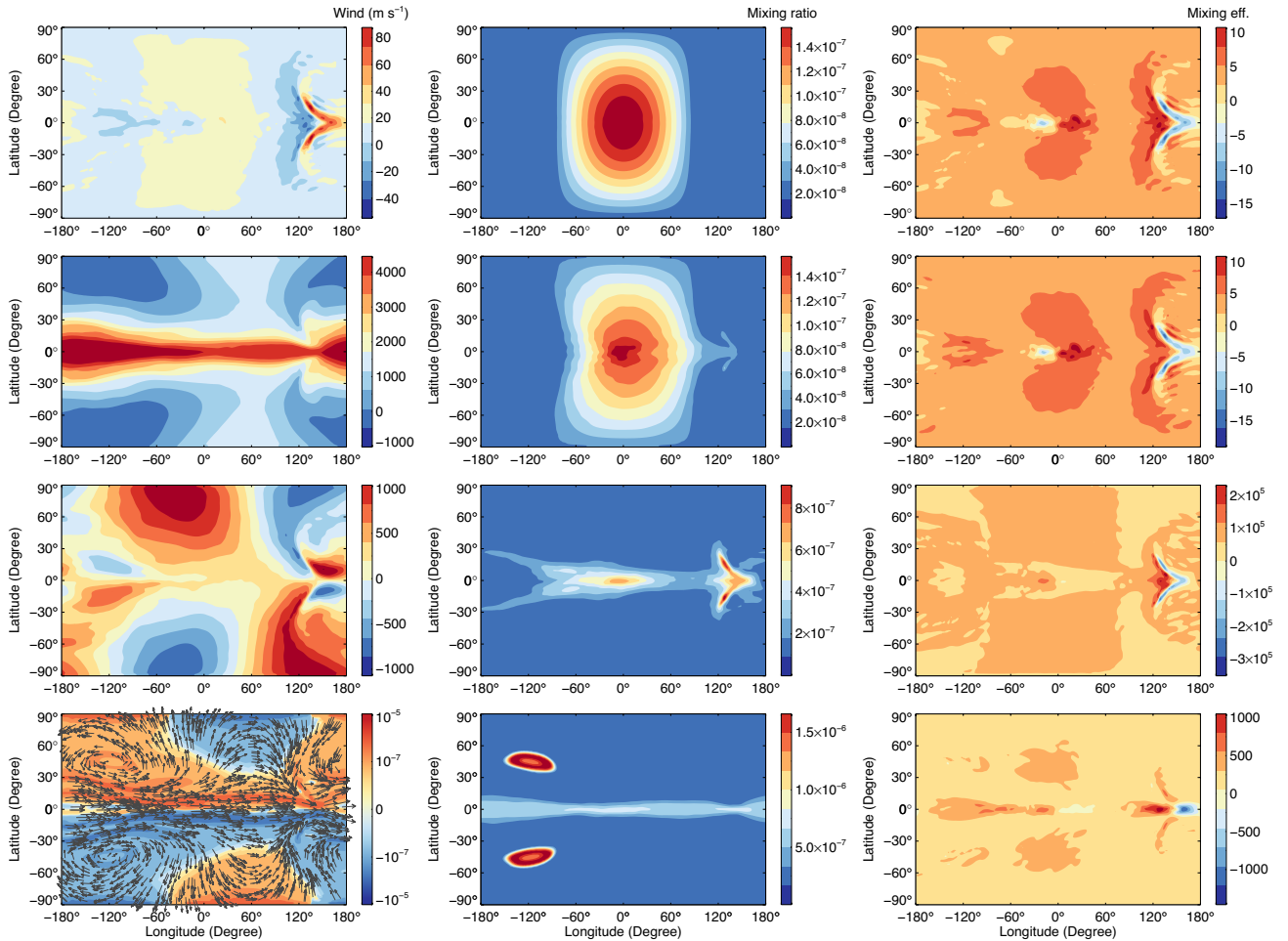


FIG. 18.— Longitude-latitude maps of various quantities at 2800 Pa in the Photochemical Experiment. Left column from top to the bottom: vertical wind (w), east-west wind (u), north-south wind (v), and relative vorticity (ζ) with wind field vectors. Central column: volume mixing ratios of tracers with chemical timescale of $10^{2.5}$ s, 10^4 s, $10^{5.5}$ s, 10^7 s from top to the bottom, respectively. Right column: corresponding vertical mixing efficiency of the tracers in the central column. Note that the color bars do not have the same range.

where local upwelling and downwelling are prominent in the vertical velocity map (Fig. 18). The very long-lived tracer ($\tau_c = 10^7$ s) is more homogeneously distributed compared with the short-lived tracers. But it exhibits two significant local anomalies, one in the northern hemisphere and the other in the southern, located between latitude 30 and 60 degrees and near longitude of west 120 degrees. The anomalies show tracer accumulations with respect to the surrounding background. Those two features might be a response to the in-situ large local wind gyres, which can be seen in the vorticity map (Fig. 18, bottom row). This more homogeneous distribution of long-lived chemical tracers across the entire globe can also be considered as a result of horizontal quenching process that briefly discussed in the Quench case (also see Cooper & Showman 2006).

The mixing efficiency in the case with non-uniform chemical equilibrium abundance is fundamentally different from the case with uniform equilibrium abundance in Section 3.2.1. The mixing efficiency of the short-lived tracers is positive everywhere on the globe, implying that the tracers are all vertically mixed in the same direction. Negative mixing efficiency appears only in the long-lived tracer regime. However, in the non-uniform chemical equilibrium abundance case, even for the very short-lived

species, mixing efficiency pattern shows large negative values in the upwelling region on the nightside (Fig. 18). This suggests that the tracers are not vertically mixed in the same direction everywhere and the global-mean vertical tracer transport is only a net difference between the upward and downward fluxes. The reason is that chemical equilibrium, instead of atmospheric dynamics, controls the spatial distribution of those short-lived chemical species. On the dayside, both the vertical velocity and tracer abundance deviation from the mean, χ'_0 , are positive, and therefore in general contribute to the upward mixing. However, on the nightside, χ'_0 is negative due to its low abundance relative to the global-mean value, anticorrelated with the positive vertical velocity. As a result, a negative mixing efficiency occurs in the upwelling region between 120 and 180 degrees in the equatorial region. Compared with the uniform chemical equilibrium abundance case (Fig. 10), those localized “chimneys” turn to “sinks” of the global-mean tracer abundance as the strong upwelling plumes transport abundant low-mixing-ratio tracers to the upper atmosphere.

Zonally averaged tracer distributions (Fig. 19) illustrate how the upper atmospheric tracers are vertically mixed into the lower atmosphere. As shown in the bottom panel of Fig. 19, the long-lived tracers are not uni-

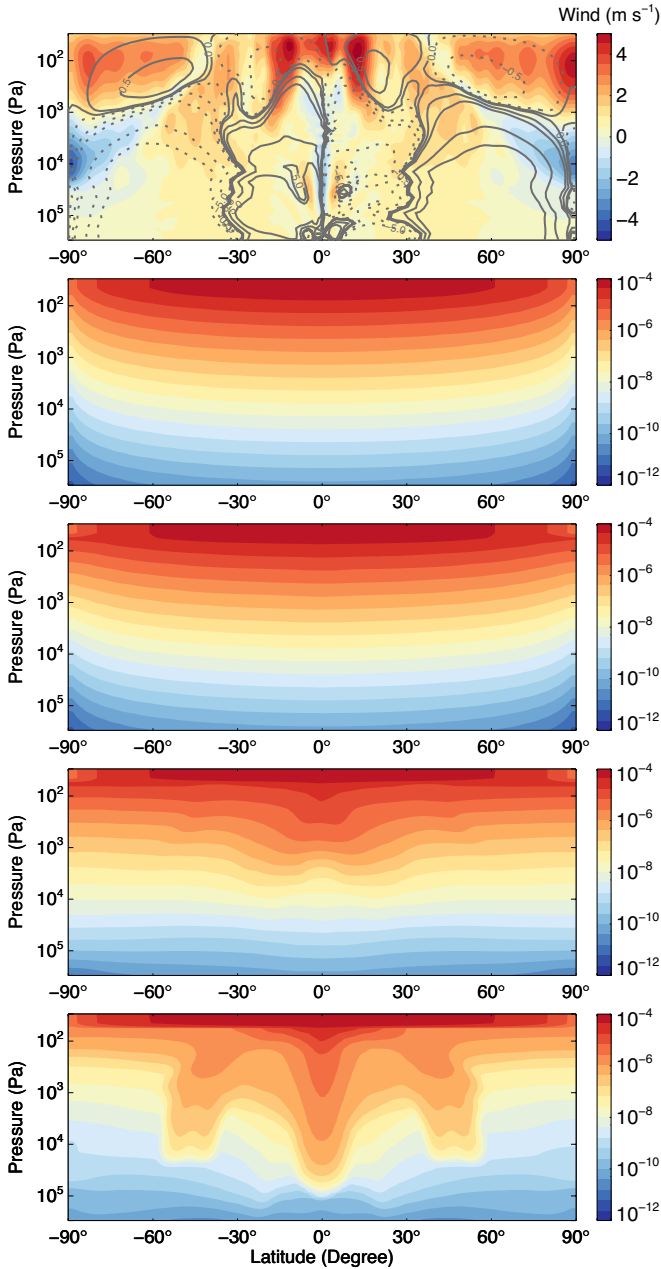


FIG. 19.— Latitude-pressure maps of zonally averaged quantities in the Photochemical Experiment. Top: vertical wind velocity (color) and TEM mass streamfunction (contours, in units of 10^{12} Kg s^{-1} , solid/positive is clockwise). Starting from the second row we show volume mixing ratio of tracers with different chemical timescales of 10^2 s, $10^{3.5}$ s, 10^5 s, $10^{6.5}$ s from top to bottom, respectively.

formly mixed downward by the circulation. Instead, the zonally averaged tracer pattern are significantly shaped by the circulation cells shown in the upper panel. Especially, at high latitudes above the 1000-Pa pressure level, the lower mixing ratio tracers from the lower atmosphere is actually circulated upward and transported to the lower latitudes by the two polar cells in the upper atmosphere. This transport leads to a decrease of the global-mean tracer mixing ratio in the upper atmosphere compared to the chemical equilibrium profile, as shown in the area-weight-mean tracer profile in Fig. 19. Only at pressure levels below 1000 Pa, the global-

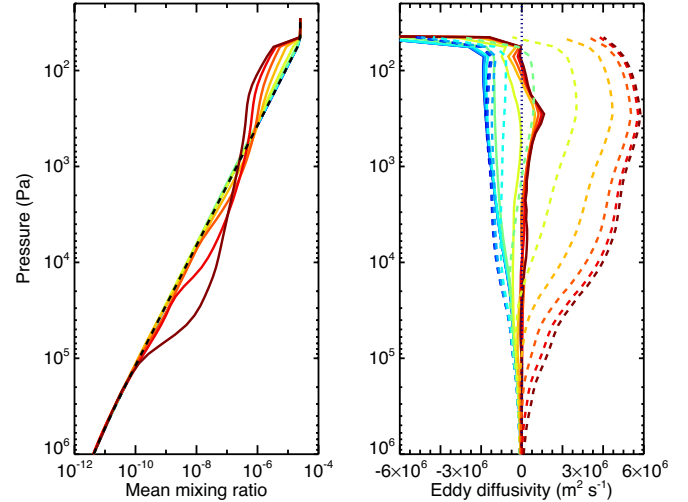


FIG. 20.— Left: vertical profiles of the global-mean volume mixing ratio in the Photochemical Experiment. Right: vertical profiles of numerically derived effective eddy diffusivity K_{eff} (right) from the flux-gradient relationship (Eq. 6) based on simulation results (solid) and that from an analytical prediction Eq. (33) (dashed) based on the root-mean-square vertical velocity scale from the simulation. Different colors from cold (blue) to warm (red) represent tracers with different chemical timescales from short to long, ranging from 10^2 s to 10^7 s.

mean tracer mixing ratio of those long-lived species becomes larger than the chemical equilibrium value. Therefore the mean tracer profile is significantly controlled by the details of the atmospheric dynamics, and there is no “quench point” in our simulations with non-uniform chemical equilibrium abundance near the top.

We found that the global-mean net vertical tracer flux of short-lived species is positive, implying that the tracer is mixed upward to the upper atmosphere. This upward transport mainly occurs in the broad upwelling region on the dayside where the tracer abundance also shows a positive anomaly (Fig. 18). Note that in this case the global-mean tracer mixing ratio is larger in the upper atmosphere where the source is located. This counter-gradient transport suggests a negative effective eddy diffusivity. We numerically derived K_{eff} based on the simulation and flux-gradient relationship (Fig. 16). It is indeed negative for short-lived species. It implies that, in the globally average sense, those tracers are mixed towards its source in the upper atmosphere, which is physically counter-intuitive in the traditional chemical-diffusion framework. However, this phenomena confirms our theory in Section 2.3.2. A significant non-diffusive component contributes to this effect, a result from the correlation between the velocity field and the equilibrium chemical distribution. If we assume the global-mean vertical profile of the tracer is not significantly different from the chemical equilibrium profile (Eq. 26), with the non-diffusive correction we introduced in Section 2.3.2, K_{eff} might still be predicted from first principles based on Eq. (15) and Eq. (26):

$$K_{eff} \approx \frac{\hat{w}^2}{\hat{w}/H + \tau_c^{-1}} - \frac{\hat{w}\Delta\chi_{eq}}{1 + \hat{w}\tau_c/H} \left(\frac{\partial\Delta\chi_{eq}}{\partial z} \right)^{-1}. \quad (37)$$

Here we have assumed that the nightside chemical equilibrium abundance χ_n is much smaller than $\Delta\chi_{eq}$. For very short-lived species ($\tau_c \rightarrow 0$), the first term on

the right hand side of Eq. (37) might be neglected, leading to a non-diffusive term only (e.g., Eq. 16):

$$K_{eff} \approx -\hat{w}\Delta\chi_{eq}\left(\frac{\partial\Delta\chi_{eq}}{\partial z}\right)^{-1}. \quad (38)$$

This expression physically explains the negative “ K_{eff} ” in the short-lived tracer simulations, even though the vertical transport is not important for those species which are mainly controlled by the local chemistry. This non-diffusive effect on the global-mean tracer transport has not been considered in current 1D models in planetary atmospheres.

Using the root-mean-square of vertical velocity \hat{w} from our simulations, we predicted K_{eff} based on Eq. (37). It qualitatively agrees with the numerically derived K_{eff} for both short-lived species and long-lived species. Eq. (37) also shows that the non-diffusive effect becomes less important than the diffusive term as the chemical timescale increases. In our simulations, the numerically derived K_{eff} increases with tracer lifetime and becomes positive for long-lived species (Fig. 20). But Eq. (37) overestimates the K_{eff} by about a factor of 5-10 in the long-lifetime regime. As noted before, if the material surface of tracer is distorted significantly, our theory in Section 2.3 is not a good predictor of the effective eddy diffusivity. Also, the assumed vertical gradient of the mean-tracer in the non-diffusive correction (Eq. 37) is not a good approximation for the long-lived tracers because the tracer distributions, both vertical and horizontal, may substantially deviate from the chemical equilibrium distribution.

It should be noted that the non-diffusive component does not always decrease K_{eff} under uniform chemical equilibrium. The sign of the non-diffusive contribution depends on the correlation between the vertical wind (w) and chemical equilibrium tracer distribution (χ'_0), as well as the vertical gradient of the global-mean tracer profile. For instance, if we consider the atmosphere region above the photochemical source layer on a tidally locked planet, chemical equilibrium abundance is large at the bottom of this region and smaller at the top, implying a negative vertical global-mean tracer gradient. In this case, the $w - \chi'_0$ correlation is still positive because the photochemical equilibrium abundance is still larger on the dayside than the nightside. But because the vertical tracer gradient is negative, the non-diffusive component will enhance the total upward global-mean tracer transport efficiency and thus K_{eff} (Eq. 37). Another example is vertical mixing of mineral cloud particles on hot Jupiter. Cloud microphysics predicts that there might be more titanium and silicate clouds forming at the west terminator region than on the nightside (e.g., Powell et al. 2017) due to colder temperature at the west limb. The spatial correlation between the vertical wind and microphysical equilibrium cloud tracer is complex in this situation and the importance of the non-diffusive contribution to K_{eff} has yet to be investigated. Moreover, cloud settling represents a qualitatively different type of source/sink than the simple linear chemical relaxation scheme that we have adopted in this paper. It is currently unclear whether such a source/sink due to particle settling would lead to diffusive behavior, even under a simplified scenario that ignores large, externally

imposed day-night variations in cloud production.

The complicated behavior of K_{eff} in the case with non-uniform chemical equilibrium abundance, especially the negative K_{eff} owing to non-diffusive effects, implies that it might be difficult to achieve a satisfactory understanding—or even a self-consistent model—of photochemical tracer transport on tidally locked exoplanets in a simple 1D framework with the same eddy diffusivity for all species. A 3D dynamical-chemical model, which might be computationally expensive, will be of a great help in revealing the underlying transport mechanisms and interactions between the chemical and dynamical processes.

4. CONCLUSION AND DISCUSSION

The central assumption in the 1D framework is that vertical tracer transport acts in a diffusive manner in a global-mean sense. Eddy diffusivity is a key parameter in this framework and is normally constrained by fitting the model to observed tracer profiles. However, the physical meaning of this empirically determined quantity is usually not elucidated, and there have been few attempts in the planetary literature to estimate it from first principles or show systematically how it should vary from planet to planet. In this study we investigated some of the fundamental processes that are lumped into—and control—this single quantity. We generalized the pioneering theoretical work from Holton (1986) on a 2D Earth model to a 3D atmosphere and explicitly derived the diffusivity expression from first principles. We performed tracer transport simulations in a 2D chemical-diffusion-advection model and a 3D GCM for both rapidly rotating planets and tidally locked planets using this same chemical source/sink scheme. By deriving the 1D eddy diffusivity from the globally averaged vertical transport flux, we showed that the simulation results in both 2D and 3D agree with our theoretical predictions. Therefore this study can serve as a theoretical foundation for future work on estimating or understanding the effective eddy diffusivity for global-mean vertical tracer transport.

The general take-home message from our investigation is that interaction between the chemistry and dynamics is important in controlling the 1D vertical tracer transport. Our work demonstrates that the global-mean vertical tracer transport crucially depends on the correlations between the vertical velocity field and the tracer horizontal variations, which is significantly modulated by atmospheric circulation, horizontal diffusion and wave mixing, and the local tracer chemistry or microphysics. Importantly, this correlation is also controlled by the chemistry itself, which implies that—even for a given atmospheric circulation—the vertical mixing rates and effective eddy diffusivity can differ from one chemical species to another. In general, we found that the traditional assumption in the current 1D models that all chemical species are transported via the same eddy diffusivity breaks down. Instead, the 1D eddy diffusivity should increase with tracer chemical lifetime and circulation strength but decrease with horizontal mixing efficiency due to breaking of Rossby waves or other horizontal mixing processes. Our analytical theory including those effects could better explain the 2D and 3D numerical simulation results in a wide parameter space. This physically motivated formulation of eddy diffusivity could be useful for future 1D

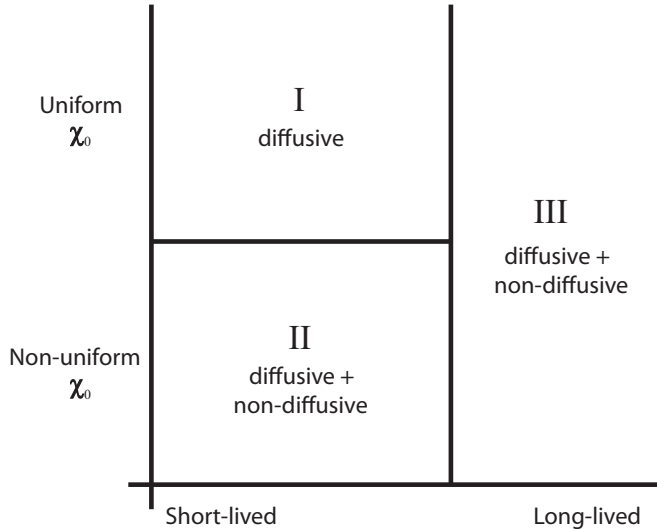


FIG. 21.— Atmospheric regimes of global-mean tracer transport as a function of tracer chemical lifetime and horizontal tracer distribution under chemical equilibrium χ_0 .

tracer transport model. Based on this new eddy diffusivity theory, we also revised the previous theory about the dynamical quenching of disequilibrium tracers.

We emphasize that the conventional “diffusive” assumption of the global-mean vertical tracer transport does not always hold. In this study we demarcated three regimes in terms of the tracer lifetime and horizontal tracer distribution under chemical equilibrium (Fig. 21). Only in regime I, a short-lived tracer with uniform distribution of chemical equilibrium abundance, the traditional diffusive assumption is mostly valid. In the other two regimes, tracer with non-uniform distribution of chemical equilibrium abundance (regime II) and the tracer lifetime significantly long compared with the transport timescale (regime III), the global-mean vertical tracer transport could be largely influenced by non-diffusive effects. Non-diffusive effects could result in a negative effective eddy diffusivity in the traditional diffusive framework, either for the short-lived species in regime II or for the long-lived species in regime III. A negative diffusivity does not physically make sense and might be difficult to incorporate into 1D models. For relatively long-lived species in regime II (but not long enough to reach regime III), we provided a simple correction term to include the non-diffusive effects, which might be useful for future 1D models.

Our detailed analytical and numerical analysis concludes several key points:

(1) Larger characteristic vertical velocities contribute to a larger global-mean tracer mixing. Everything else being equal (in particular, if there are no huge variations in chemical timescales with height), this then implies that, if the vertical velocity increases with height, the eddy diffusivity also increases with the height in the atmosphere. For short-lived tracers in regime I, $K_{eff} \propto \hat{w}^2$ and for the long-lived tracers in all regimes, $K_{eff} \propto \hat{w}$ if the non-diffusive effect is not significant.

(2) Efficient horizontal eddy mixing due to breaking of Rossby waves or other wave processes will smooth out the horizontal variations of tracer and thus decrease the global-mean eddy diffusivity. But the horizontal tracer advection due to the mean flow can either increase or de-

crease the eddy diffusivity, depending on the eddy tracer flux convergence/divergence induced by the mean flow, which fundamentally depends on the correlation between the horizontal mean flow and the horizontal tracer variations.

(3) Global-mean eddy diffusivity depends on the tracer sources and sinks due to chemistry and microphysics. In an idealized case with linear chemical relaxation, we showed that the effective eddy diffusivity increases with the chemical relaxation timescale (i.e., chemical lifetime). In regime I, $K_{eff} \propto \tau_c$. When the chemical lifetime is very long (regime III), the effective eddy diffusivity reaches its asymptotic value—a product of vertical wind velocity and vertical transport length scale.

(4) In regime I, short-lived species exhibit a similar spatial pattern as the vertical velocity field (as viewed on an isobar). But if the equilibrium chemical field has horizontal variations (regime II), the resulting tracer distribution is complicated. In regime III, the pattern of a long-lived tracer is largely controlled by the atmospheric dynamics. In this case, the correlation between vertical velocity and tracer fields (on isobars) breaks down, and the vertical profile of the tracer abundance differs substantially from its chemical equilibrium profile. The horizontal variation of the long-lived tracers is generally smaller than that of the short-lived tracers due to horizontal mixing. If the tracer lifetime is sufficiently long (i.e., $\tau_c \rightarrow \infty$), the horizontal tracer field is expected to be completely homogenized across the globe, but we did not simulate this physical limit in this study.

(5) The diffusive assumption is generally valid in regime I and the effective eddy diffusivity is always positive using our idealized chemical schemes. But in regime II, there is a strong variation in the equilibrium chemical field. Non-diffusive effects are important in regime II if there is a good correlation between the equilibrium tracer field and the vertical velocity field. In some situations, tracers could be vertically mixed towards the source in a global-mean sense, leading to a negative eddy diffusivity. As the chemical lifetime increases in regime II (but not long enough to reach regime III), the non-diffusive effect could become less significant.

(6) Non-diffusive behavior could occur in regime III when the tracer chemical lifetime is much longer than the atmospheric dynamical timescale. In this regime, the tracer material surface is distorted significantly and the global-mean tracer profile is complicated. For example, in the case where the tracer source is in the deep atmosphere, the global-mean tracer profile could exhibit a local minimum in the middle atmospheric layers. The derived effective eddy diffusivity will be negative above the local minimum, suggesting a strong non-diffusive effect.

(7) We derived the analytical species-dependent eddy diffusivity for tracers with uniform chemical equilibrium (Eq. 13). We also provided a simple non-diffusive correction for long-lived tracers with non-uniform chemical equilibrium (Eq. 15). The dynamical timescale in our theory depends on the horizontal length scale L_h and/or vertical length scale L_v of the tracer transport. Using the pressure scale height H as L_v , the theoretical predictions generally agree with our 2D and 3D numerical simulations. For long-lived species, the actual L_v appears larger than H in our 2D simulations but smaller

than H in the 3D tidally locked exoplanet cases.

(8) A widely accepted assumption in current 1-D chemical models of planetary atmospheres—species-independent eddy diffusion, which assumes a single profile of vertical eddy diffusivity for all species—is generally invalid. Using a species-dependent eddy diffusivity in our theory will lead to a more realistic understanding of global-mean tracer transport in planetary atmospheres. For example, it seems difficult to simultaneously fit the vertical profiles of both C_2H_2 and C_2H_6 in the stratosphere of Neptune (Moses et al. 2005). As the chemistry of the two species is relatively well known and the chemical lifetimes of them differ by a factor of 100 or more (Zhang et al. 2013a), the effective eddy diffusivities acting on them should be different.

(9) Based on the species-dependent eddy diffusivity theory, we provide a new analytical theory of the global-mean departure “quench” point of the tracer from its chemical equilibrium profile. Because the species-dependent eddy diffusivity is smaller than the conventional species-independent value, the departure point estimated in our theory is located at lower pressure than the previous estimate if the tracer chemical timescale increases with decreasing pressure. For tracers on close-in tidally locked exoplanets, the departure point estimated from our theory assuming $L_v \sim H$ agrees with the numerical simulations for longer-live species. For shorter-lived species, using the equilibrium chemical scale height H_{ceq} as L_v provides a better estimate.

How to better approximate the 3D tracer transport in a 1D model for real atmospheres? We emphasize that it is the correlation between the 2D tracer fields and 2D vertical velocity field along an isobar that determines the vertical transport efficiency. Here we propose two approaches. First, from a theoretical point of view, it is necessary to perform 3D tracer transport simulations with some simplified chemical and microphysical schemes for a specific atmospheric situation and analyze how to better parameterize the 1D effective tracer transport in that atmospheric regime. Taking close-in tidally locked planets as an example, one could include simplified dayside photochemistry and ion chemistry to study a chemically active species, and/or include nightside haze/cloud condensation and dayside particle evaporation to study cloud particle transport. Parmentier et al. (2013) and this study represent an initial step in this direction.

Second, from an observational point of view, it would be interesting to perform a correlation analysis between

the observed 2D tracer fields and the vertical velocity field (or the simulated vertical velocity field if the vertical velocity is not easy to determined from observations). Even for exoplanets, observations are starting to reveal horizontal gas distributions (Stevenson et al. 2017) and the cloud distribution from the light curve data (e.g., Parmentier et al. 2016). A correlation analysis between the tracer fields and the velocity field estimated from the atmospheric models (e.g., Dobbs-Dixon & Lin 2008; Showman et al. 2009; Rauscher & Menou 2010; Heng et al. 2011; Perna et al. 2010; Mayne et al. 2014) may shed lights on how the vertical tracer transport works on those planets and lead to a better understanding of global-mean vertical eddy mixing for future chemical models and cloud models.

Finally, we should note that, in this study we only focused on idealized chemical schemes that relax the tracer distribution toward a specified chemical equilibrium over a specified timescale. Other types of sources/sinks, for instance, due to cloud particle setting or due to more complex gas-phase chemistry have yet to be explored. The global-mean vertical transport behaviors of those tracers are worth to investigate in the future. Furthermore, besides the larger-scale upwelling and downwelling transport, waves might also contribute to the vertical mixing in the stratified atmosphere although we did not focus that effect in this study. In the high atmosphere such as mesosphere on Earth or thermosphere on Jupiter, gravity waves could lead to a strong tracer mixing. Lindzen (1981) first proposed that the gravity wave breaking including the breaking of tidal waves will significantly mix the tracers vertically. Even without gravity wave breaking, Strobel (1981) considered the tracer transport by linear gravity waves. A further theory in Schoeberl & Strobel (1984) proposed parameterization including both gravity wave breaking and tracer mixing by linear waves. Strobel et al. (1987) also found that the effective vertical eddy diffusivity due to gravity waves depends on the tracer chemical lifetime. It is expected that the total vertical eddy diffusivity would be a sum of both larger scale mixing and gravity wave mixing. A further investigation is needed so that the 1D vertical tracer transport can be understood in a coherent 3D chemical-transport framework from the deep, turbulent atmosphere to the upper, low-density atmosphere including convective mixing, large-scale circulation, mixing from atmospheric wave processes such as breaking of Rossby waves and gravity waves.

APPENDIX

DERIVATION OF 1D EFFECTIVE EDDY DIFFUSIVITY IN A 2D CHEMICAL-ADVECTIVE-DIFFUSIVE SYSTEM

The governing tracer transport equation of a 2D chemical-advection-diffusive system using the coordinates of log-pressure and latitude is (Eq. 19 in the text, Shia et al. 1989, Shia et al. 1990, Zhang et al. 2013b):

$$\frac{\partial \chi}{\partial t} + v^* \frac{\partial \chi}{\partial y} + w^* \frac{\partial \chi}{\partial z} - \frac{1}{\cos \phi} \frac{\partial}{\partial y} (\cos \phi K_{yy} \frac{\partial \chi}{\partial y}) - e^{z/H} \frac{\partial}{\partial z} (e^{-z/H} K_{zz} \frac{\partial \chi}{\partial z}) = S \quad (\text{A.1})$$

where χ is the tracer mixing ratio, $\phi = y/R$ is latitude and R is the planetary radius. $z \equiv -H \log(p/p_0)$ is the log-pressure coordinate, where H is a constant reference scale height, p is pressure and p_0 is the pressure at the bottom boundary. K_{yy} and K_{zz} are the horizontal and vertical eddy diffusivities, respectively. Residual circulation velocities are v^* and w^* in the meridional and vertical directions, respectively. A mass streamfunction ψ can be introduced such that:

$$v^* = -\frac{1}{2\pi a \rho_0 \cos \phi} e^{z/H} \frac{\partial}{\partial z} (e^{-z/H} \psi) \quad (\text{A.2a})$$

$$w^* = \frac{1}{2\pi a \rho_0 \cos \phi} \frac{\partial \psi}{\partial y} \quad (\text{A.2b})$$

where ρ_0 is the reference density of the atmosphere at log-pressure $z = 0$. The v^* and w^* given in Eq. (A.2) naturally satisfy the continuity equation:

$$\frac{1}{\cos \phi} \frac{\partial}{\partial y} (\cos \phi v^*) + e^{z/H} \frac{\partial}{\partial z} (e^{-z/H} w^*) = 0. \quad (\text{A.3})$$

Combining Eq. (A.1) and Eq. (A.3), we obtain the flux form of the tracer transport equation:

$$\frac{\partial \chi}{\partial t} + \frac{1}{\cos \phi} \frac{\partial}{\partial y} (\cos \phi v^* \chi) + e^{z/H} \frac{\partial}{\partial z} (e^{-z/H} w^* \chi) - \frac{1}{\cos \phi} \frac{\partial}{\partial y} (\cos \phi K_{yy} \frac{\partial \chi}{\partial y}) - e^{z/H} \frac{\partial}{\partial z} (e^{-z/H} K_{zz} \frac{\partial \chi}{\partial z}) = S. \quad (\text{A.4})$$

Here we also define the eddy-mean decomposition $A = \bar{A} + A'$ where \bar{A} is the latitudinally averaged quantity at constant pressure and A' is the eddy term. Taking the latitudinal average of Eq. (A.3) to eliminate the meridional transport term (the v^* term), we obtain $\overline{w^*} = 0$ at isobars if we assume the latitudinal-mean vertical velocity $\overline{w^*}$ vanishes at top and bottom boundaries. We average Eq. (A.4) and both meridional advection and diffusion terms vanish. Using $\overline{w^*} = 0$, we obtain:

$$\frac{\partial \bar{\chi}}{\partial t} + e^{z/H} \frac{\partial}{\partial z} (e^{-z/H} \overline{w^* \chi'}) - e^{z/H} \frac{\partial}{\partial z} (e^{-z/H} K_{zz} \frac{\partial \bar{\chi}}{\partial z}) = \bar{S}. \quad (\text{A.5})$$

Based on the ‘‘flux-gradient relationship’’, we can introduce an eddy diffusivity K_w to approximate the vertical transport term associated with w^* (the second term in the left hand side) such that:

$$\overline{w^* \chi'} \approx -K_w \frac{\partial \bar{\chi}}{\partial z}. \quad (\text{A.6})$$

Then the 1D global-mean tracer transport equation (Eq. A.5) can be formulated as a vertical diffusion equation:

$$\frac{\partial \bar{\chi}}{\partial t} - e^{z/H} \frac{\partial}{\partial z} (e^{-z/H} K_{eff} \frac{\partial \bar{\chi}}{\partial z}) = \bar{S} \quad (\text{A.7})$$

where define the total 1D effective eddy diffusivity $K_{eff} = K_w + K_{zz}$. Therefore, the K_{zz} vertical eddy diffusion term in Eq. (A.5) can be treated as an additive term in the total global-mean effective eddy diffusivity K_{eff} .

In order to analytically derive K_w , we subtract both Eq. (A.5) and Eq. (A.3) multiplied by $\bar{\chi}$ from Eq. (A.4):

$$\frac{\partial \chi'}{\partial t} + \frac{1}{\cos \phi} \frac{\partial}{\partial y} (\cos \phi v^* \chi') - \frac{1}{\cos \phi} \frac{\partial}{\partial y} (\cos \phi K_{yy} \frac{\partial \chi'}{\partial y}) + w^* \frac{\partial \bar{\chi}}{\partial z} + e^{z/H} \frac{\partial}{\partial z} [e^{-z/H} (w \chi' - \overline{w^* \chi'} - K_{zz} \frac{\partial \chi'}{\partial z})] = S'. \quad (\text{A.8})$$

To solve this equation for χ' , we made four assumptions that are similar to those in Section 2.3.

- (i) We neglect the first temporal evolution term in statistical steady state.
- (ii) We neglect the complicated eddy term (the fifth term) by assuming the vertical transport of the tracer eddy χ' is much smaller than that of the latitudinal-mean tracer ($\bar{\chi}$, the fourth term). Here we have also assumed the vertical diffusion of χ' (the K_{zz} term) is much smaller than than the vertical advection of the mean tracer.
- (iii) We approximate the horizontal tracer eddy flux terms (second and third terms) in a linear relaxation form. In Section 2.3, we have decomposed the horizontal mixing processes in a 3D atmosphere into the tracer advection by zonal-mean flow and the tracer diffusion by horizontal eddies and waves. In the zonal-mean 2D system, the second and third terms in the left hand side of Eq. (A.8) correspond to the advection and diffusion process, respectively. For the advection term, we have:

$$\frac{1}{\cos \phi} \frac{\partial}{\partial y} (\cos \phi v^* \chi') \approx \frac{\chi'}{\tau_{adv}} \quad (\text{A.9})$$

where $\tau_{adv} \approx L_h / \hat{v}^*$ where L_h is the horizontal length scale and \hat{v}^* is the meridional velocity scale. From the continuity equation (Eq. A.3), we can also show $\tau_{adv} \approx L_v / \hat{w}^*$, where L_v is the vertical length scale and \hat{w}^* is the vertical velocity scale. Similarly, the diffusive term can be approximated as:

$$- \frac{1}{\cos \phi} \frac{\partial}{\partial y} (\cos \phi K_{yy} \frac{\partial \chi'}{\partial y}) \approx \frac{\chi'}{\tau_{diff}} \quad (\text{A.10})$$

where $\tau_{diff} \approx a^2 / K_{yy}$. Here we have made an additional assumption that the positive tracer anomaly ($\chi' > 0$) is associated with the tracer eddy flux divergence (i.e., the sign of the left hand side is positive in this situation) and the negative anomaly is associated with the tracer eddy flux convergence. This is generally a good assumption as long as the material surface of the tracer is not very complicated. For example, if the horizontal tracer distribution can be approximated by a second-degree Legendre polynomial as in Holton (1986), one can show that our above argument holds true.

(iv) We also consider a linear chemical scheme which relaxes the tracer distribution towards local chemical equilibrium χ_0 in a timescale τ_c . After the mean-eddy decomposition, we obtain the latitudinal mean of the chemical source/sink term $\bar{S} = (\overline{\chi_0} - \bar{\chi})/\tau_c$ and the departure $S' = (\chi'_0 - \chi')/\tau_c$. See Section 2.3 for details.

With above assumptions, Eq. (A.8) can be simplified as:

$$w^* \frac{\partial \bar{\chi}}{\partial z} + \frac{\chi'}{\tau_{adv}} + \frac{\chi'}{\tau_{diff}} = \frac{\chi'_0 - \chi'}{\tau_c}. \quad (\text{A.11})$$

We solve for χ' :

$$\chi' = \frac{-w^* \frac{\partial \bar{\chi}}{\partial z} + \tau_c^{-1} \chi'_0}{\tau_{diff}^{-1} + \tau_{adv}^{-1} + \tau_c^{-1}}. \quad (\text{A.12})$$

Inserting Eq. (A.12) in Eq. (A.6), we solve for K_w and finally obtain the analytical expression for K_{eff} :

$$K_{eff} \approx K_{zz} + \frac{\overline{w^{*2}}}{\tau_{diff}^{-1} + \tau_{adv}^{-1} + \tau_c^{-1}} - \frac{\overline{w^* \chi'_0}}{1 + \tau_{diff}^{-1} \tau_c + \tau_{adv}^{-1} \tau_c} \left(\frac{\partial \bar{\chi}}{\partial z} \right)^{-1} \quad (\text{A.13})$$

In our 2D system study (Section 3.1), we have assumed that the chemical equilibrium abundance is uniformly distributed across the latitude. That implies χ'_0 is zero and thus the last term in the right hand side vanishes. Given the specific meridional circulation patterns in Eq. (20), the area-weighted global-mean vertical velocity scale is $\hat{w}^* = \gamma w_0 e^{\eta z/H}$. Assuming the horizontal transport length scale L_h is the planetary radius a and vertical transport length scale L_v is the pressure scale height H , we predict K_{eff} for our 2D cases (Eq. 22 in the text):

$$K_{eff} \approx K_{zz} + \frac{\gamma^2 w_0^2 e^{2\eta z/H}}{K_{yy} a^{-2} + \gamma w_0 e^{\eta z/H} H^{-1} + \tau_c^{-1}}. \quad (\text{A.14})$$

ACKNOWLEDGEMENTS

This research was supported by NASA Solar System Workings Grant NNX16AG08G to X.Z. and A.P.S.. We thank T. Komacek, V. Parametier and X. Tan for helpful discussions. We thank Y. Yung, R. Shia, and J. Moses for providing the eddy diffusion profiles in their JPL/kinetics chemical models. Some of the simulations were performed on the Stampede supercomputer at TACC through an allocation by XSEDE.

REFERENCES

- Ackerman, A. S., & Marley, M. S. 2001, *ApJ*, 556, 872
 Adcroft, A., Campin, J.-M., Hill, C., & Marshall, J. 2004, *Monthly Weather Review*, 132, 2845
 Allen, M., Yung, Y. L., & Waters, J. W. 1981, *Journal of Geophysical Research: Space Physics*, 86, 3617
 Andrews, D., & McIntyre, M. E. 1976, *Journal of the Atmospheric Sciences*, 33, 2031
 Andrews, D. G., Holton, J. R., & Leovy, C. B. 1987, *Middle atmosphere dynamics No. 40* (Academic press)
 Bordwell, B., Brown, B. P., & Oishi, J. S. 2018, *The Astrophysical Journal*, 854, 8
 Bougher, S. W., Hunten, D. M., & Phillips, R. J. 1997, *Venus II—geology, Geophysics, Atmosphere, and Solar Wind Environment, Vol. 1* (University of Arizona Press)
 Charnay, B., Meadows, V., & Leconte, J. 2015a, arXiv preprint arXiv:1509.06814
 Charnay, B., Meadows, V., Misra, A., Leconte, J., & Arney, G. 2015b, arXiv preprint arXiv:1510.01706
 Cooper, C. S., & Showman, A. P. 2005, *ApJ*, 629, L45
 —. 2006, *ApJ*, 649, 1048
 Dobbs-Dixon, I., & Lin, D. N. C. 2008, *ApJ*, 673, 513
 Drummond, B., Mayne, N., Baraffe, I., et al. 2018, arXiv preprint arXiv:1801.01045
 Gao, P., & Benneke, B. 2016, in *AAS/Division for Planetary Sciences Meeting Abstracts, Vol. 48*
 Gao, P., Zhang, X., Crisp, D., Bardeen, C. G., & Yung, Y. L. 2014, *Icarus*, 231, 83
 Garcia, R. R., & Solomon, S. 1983, *Journal of Geophysical Research: Oceans*, 88, 1379
 Helling, C., Woitke, P., & Thi, W.-F. 2008, *Astronomy & Astrophysics*, 485, 547
 Heng, K., Menou, K., & Phillipps, P. J. 2011, *MNRAS*, 413, 2380
 Holton, J. R. 1986, *Journal of Geophysical Research: Atmospheres*, 91, 2681
 Hu, R., Seager, S., & Bains, W. 2012, *The Astrophysical Journal*, 761, 166
 Hunten, D. M. 1975, in *Atmospheres of Earth and the Planets* (Springer), 59–72
 Kataria, T., Showman, A. P., Fortney, J. J., Marley, M. S., & Freedman, R. S. 2014, *ApJ*, 785, 92
 Knutson, H. A., Charbonneau, D., Allen, L. E., et al. 2007, *Nature*, 447, 183
 Komacek, T. D., & Showman, A. P. 2016, *The Astrophysical Journal*, 821, 16
 Krasnopolsky, V., & Parshev, V. 1981, *Nature*, 292, 610
 Lavvas, P., Coustenis, A., & Vardavas, I. 2008, *Planetary and Space Science*, 56, 27
 Lee, G., Dobbs-Dixon, I., Helling, C., Bognar, K., & Woitke, P. 2016, *Astronomy & Astrophysics*, 594, A48
 Lefèvre, F., Lebonnois, S., Montmessin, F., & Forget, F. 2004, *Journal of Geophysical Research: Planets*, 109
 Lefèvre, F., Bertaux, J.-L., Clancy, R. T., et al. 2008, *Nature*, 454, 971
 Lewis, N. K., Showman, A. P., Fortney, J. J., et al. 2010, *ApJ*, 720, 344
 Li, C., Zhang, X., Gao, P., & Yung, Y. 2015, *The Astrophysical Journal Letters*, 803, L19
 Li, J., & Goodman, J. 2010, *ApJ*, 725, 1146
 Lian, Y., & Showman, A. P. 2010, *Icarus*, 207, 373
 Lindzen, R. S. 1981, *Journal of Geophysical Research: Oceans*, 86, 9707
 Line, M. R., Vasisht, G., Chen, P., Angerhausen, D., & Yung, Y. L. 2011, *The Astrophysical Journal*, 738, 32
 Liu, B., & Showman, A. P. 2013, *ApJ*, 770, 42
 Marcq, E., & Lebonnois, S. 2013, *Journal of Geophysical Research: Planets*, 118, 1983
 Mayne, N. J., Baraffe, I., Acreman, D. M., et al. 2014, *Astronomy & Astrophysics*, 561, A1

- Moses, J., Fouchet, T., Bézard, B., et al. 2005, *Journal of Geophysical Research: Planets*, 110
- Moses, J. I., & Poppe, A. R. 2017, *Icarus*, 297, 33
- Moses, J. I., Visscher, C., Fortney, J. J., et al. 2011, *ApJ*, 737, 15
- Moses, J. I., Line, M. R., Visscher, C., et al. 2013, *The Astrophysical Journal*, 777, 34
- Nair, H., Allen, M., Anbar, A. D., Yung, Y. L., & Clancy, R. T. 1994, *Icarus*, 111, 124
- Nixon, C. A., Achterberg, R. K., Romani, P. N., et al. 2010, *Planetary and Space Science*, 58, 1667
- Parmentier, V., Fortney, J. J., Showman, A. P., Morley, C., & Marley, M. S. 2016, *The Astrophysical Journal*, 828, 22
- Parmentier, V., Showman, A. P., & Lian, Y. 2013, *Astronomy & Astrophysics*, 558, A91
- Perna, R., Menou, K., & Rauscher, E. 2010, *ApJ*, 719, 1421
- Plumb, R., & Mahlman, J. 1987, *Journal of the atmospheric sciences*, 44, 298
- Powell, D., Zhang, X., Gao, P., & Parmentier, V. 2017, in *American Astronomical Society Meeting Abstracts*, Vol. 229
- Prandtl, L. 1925, *Zeitschrift fur angew. Math. u. Mechanik*, 5, 136
- Prather, M. J. 1986, *Journal of Geophysical Research: Atmospheres*, 91, 6671
- Prinn, R., & Owen, T. 1976, in *IAU Colloq. 30: Jupiter: Studies of the Interior, Atmosphere, Magnetosphere and Satellites*, 319–371
- Prinn, R. G., & Barshay, S. S. 1977, *Science*, 198, 1031
- Rauscher, E., & Menou, K. 2010, *ApJ*, 714, 1334
- Schoeberl, M. R., & Strobel, D. F. 1984, *Dynamics of the Middle Atmosphere*, 45
- Shia, R.-L., Ha, Y. L., Wen, J.-S., & Yung, Y. L. 1990, *Journal of Geophysical Research: Atmospheres*, 95, 7467
- Shia, R.-L., Yung, Y. L., Allen, M., Zurek, R. W., & Crisp, D. 1989, *Journal of Geophysical Research: Atmospheres*, 94, 18467
- Showman, A. P., Fortney, J. J., Lewis, N. K., & Shabram, M. 2013, *ApJ*, 762, 24
- Showman, A. P., Fortney, J. J., Lian, Y., et al. 2009, *ApJ*, 699, 564
- Showman, A. P., & Guillot, T. 2002, *A&A*, 385, 166
- Smith, M. D. 1998, *Icarus*, 132, 176
- Stevenson, K. B., Line, M. R., Bean, J. L., et al. 2017, *The Astronomical Journal*, 153, 68
- Stolzenbach, A., Lefèvre, F., Lebonnois, S., Maattanen, A., & Bekki, S. 2015, in *AGU Fall Meeting Abstracts*
- Strobel, D. F. 1981, *Journal of Geophysical Research: Oceans*, 86, 9806
- Strobel, D. F., Summers, M. E., Bevilacqua, R. M., DeLand, M. T., & Allen, M. 1987, *Journal of Geophysical Research: Atmospheres*, 92, 6691
- Tsai, S.-M., Lyons, J. R., Grosheintz, L., et al. 2017, *The Astrophysical Journal Supplement Series*, 228, 20
- Tung, K. K. 1982, *Journal of the Atmospheric Sciences*, 39, 2330
- Turco, R., Hamill, P., Toon, O., Whitten, R., & Kiang, C. 1979, *Journal of the Atmospheric Sciences*, 36, 699
- Visscher, C., & Moses, J. I. 2011, *ApJ*, 738, 72
- Wong, M. L., Fan, S., Gao, P., et al. 2017, *Icarus*, 287, 110
- Youdin, A. N., & Mitchell, J. L. 2010, *The Astrophysical Journal*, 721, 1113
- Yung, Y. L., Allen, M., & Pinto, J. P. 1984, *The Astrophysical Journal Supplement Series*, 55, 465
- Zhang, X., Liang, M. C., Mills, F. P., Belyaev, D. A., & Yung, Y. L. 2012, *Icarus*, 217, 714
- Zhang, X., Nixon, C., Shia, R., et al. 2013a, *Planetary and Space Science*, 88, 3
- Zhang, X., Shia, R.-L., & Yung, Y. L. 2013b, *The Astrophysical Journal*, 767, 172
- Zhang, X., & Showman, A. P. 2017, *The Astrophysical Journal*, 836, 73